Feasibility of Tomography with Unknown View Angles

Samit Basu, *Member, IEEE,* and Yoram Bresler, *Fellow, IEEE*

***Abstract*—In the standard two-dimensional (2-D) parallel beam tomographic formulation, it is generally assumed that the angles at which the projections were acquired are known. We have recently demonstrated, however, that under fairly mild conditions these view angles can be uniquely recovered from the projections themselves. In this paper, we address the question of reliability of such solutions to the angle recovery problem using moments of the projections. We demonstrate that under mild conditions, the angle recovery problem has unique solutions and is stable with respect to perturbations in the data. Furthermore, we determine the Cramér-Rao lower bounds on the variance of the estimates of the angles when the projection are corrupted by additive Gaussian noise. We also treat the case in which each projection is shifted by some unknown amount which must be jointly estimated with the view angles. Motivated by the stability results and relatively small values of the error bounds, we construct a simple algorithm to approximate the ML estimator and demonstrate that the problem can be feasibly solved in the presence of noise. Simulations using this simple estimator on a variety of phantoms show excellent performance at low to moderate noise levels, essentially achieving the Cramér–Rao bounds.**

***Index Terms*—Feasibility, motion, stability, tomography, unknown view angle.**

I. Introduction

In its traditional formulation, computerized tomography is the reconstruction of an object from measurements that are line integrals of that object at some set of *known* orientations, referred to as *view angles*. This formulation has found a wide variety of applications including medical imaging, nondestructive testing, synthetic aperture radar (SAR), and electron-microscopy-based tomography among others [1]. In the case of two-dimensional (2-D) parallel beam projection tomography, however, we have recently demonstrated that under some fairly general conditions the view angles are in fact uniquely determined by the projection data [2]. If the angles can be reliably determined from the projection data in the presence of measurement noise, then it becomes possible to apply tomographic principles to more general data collection scenarios. In medical imaging, for example, involuntary patient motion can result in uncertainty as to the true view angles, as well as unknown shifts in the projections. A related problem arises in reconstructing a three-dimensional (3-D) model of a virus from a single projection of many identical units at random orientations in a substrate.

The problem of unknown view angles has been addressed in various limited contexts. In the case of magnetic resonance imaging (MRI), for example, a good deal of work has been done on studying and overcoming specific types of uncontrollable patient motion [3]–[6]. The uniqueness issues have been addressed in [2], and the moment based approach to finding the view angles from the projection data have been examined in [7] and [8]. What we present in this work is of a fundamentally different nature, in that we study the issues of stability of the view angle estimation problem with noisy projection data. These results allow us to characterize the feasibility of solving the view angle recovery problem in a practical setting. Furthermore, we also take the additional step of demonstrating how errors in the view angle estimates can be propagated to the reconstruction, thus characterizing the types of distortions that can occur when the view angles are estimated from the projection data.

The paper is organized as follows. The problem is formulated, and some fundamental quantities defined, along with a brief review of the principles of tomography in Section II. In Section II, we also define the problem of recovering the view angles and discuss equivalence of solutions to the angle recovery problem. In Section III, we introduce the notion of stability as considered in this paper. We also state the main results of the work: for almost all objects, under some mild conditions, the angle recovery problem can be uniquely and reliably solved in the presence of noise. A similar result holds for the case in which the projections are shifted by an unknown amount as well. Section IV derives conditions for stability of the problem of recovering the view angles (and the shifts) from the projection data. In Section V, additional bounds are calculated, demonstrating, for example, how errors in the view angle estimates propagate through a convolution backprojection (CBP) reconstruction, and how the MLE and CRB behave as the number of projection moments used is increased. In Section VI, we demonstrate feasibility of solution by constructing a simple estimator for the view angles, and comparing its performance with the bounds developed previously. Conclusions are discussed in Section VII.

II. Problem Formulation

In this section, we briefly review the Radon transform, and then introduce the problem of angle recovery. Detailed descriptions of the tomographic problem can be found in many sources, including [1], [9] and the references therein. We consider the imaging of objects f that are elements of the space $L_2(\mathbb{B}_2)$ of

Manuscript received March 27, 1998; revised May 21, 1999. This work was supported in part by the National Science Foundation under Grants MIP 91-57377 and CDA 96-24396 and a Fellowship from the Joint Services Electronics Program. The associate editor coordinating the review of this manuscript and approving it for publication was Prof. Jeffrey A. Fessler.

S. Basu is with General Electric Corporate Research and Development Center, Niskayuna, NY 12309 USA (e-mail: basu@crd.ge.com).

Y. Bresler is with the Coordinated Science Laboratory, University of Illinois at Urbana-Champaign, Urbana, IL 61801 USA (e-mail: ybresler@uiuc.edu).

Publisher Item Identifier S 1057-7149(00)04866-1.

square integrable real-valued functions[1] supported on the closed unit ball $\mathbb{B}_2$ in the plane. Parallel-beam line integral projections of f are acquired at view angles in the range $\Omega \triangleq [-\pi, \pi]$. We consider the reconstruction of f from a set of P of these projections, taken at view angles $\theta_i, i \in I \triangleq \{1, \cdots, P\}$, the components of the vector $\boldsymbol{\theta} \in \Omega^P \triangleq [-\pi, \pi]^P$. Such a set of projections, known as a sinogram, is an element of $\{L_2(\mathbb{B})\}^P$, the P-wise Cartesian product of L_2 real-valued functions supported on the interval $\mathbb{B} = [-1, 1]$. The sinogram, in turn, is related to the original image by the discrete-angle Radon transform operator $\mathcal{R}_\theta$:$L_2(\mathbb{B}_2) \rightarrow \{L_2(\mathbb{B})\}^P$ as $g = \mathcal{R}_\theta f$, where each of the P projections, defined by

$$\mathcal{R}_\theta f(s, i) = \int f(s\cos\theta_i - t\sin\theta_i, s\sin\theta_i + t\cos\theta_i)\, dt \quad (1)$$

for $s \in [-1, 1]$, corresponds to the collection of line integrals through f in the direction perpendicular to θ_i.

As in [2], we will assume that the view angles are π-*distinct*, i.e., that $|\theta_i - \theta_j| \neq \pi$ for any $i, j \in I$. This assumption ensures that projections at different view angles are not trivially related. More specifically, suppose $\theta_i = \theta_j + \pi$ for some $i \neq j \in I$. Then $g(s, i) = g(-s, j)$ follows directly from (1). Hence, projections at angles that are not π-distinct do not constitute "new" information.

We will address the following two problems:

Definition 1: [Angle Recovery Problem (ARP)]. Given a set of P projections, determine the angles θ_i at which they were acquired.

Definition 2: [Shift-angle Recovery Problem (SHARP)]. Given a set of P projections, each shifted by some unknown amount, determine the shifts, and solve the ARP.

Some immediate difficulties arise in attempting to characterize solutions to the ARP and SHARP. As discussed in [2], any set of P projections at unknown view angles, can at best determine the object f to within an orthogonal transformation, i.e., a rotation through some angle, plus a possible reflection about some axis through the origin in the plane of the object. Similarly, in the case of the SHARP, translates of the original object will yield sets of projections which are shifted in some unknown way. Hence, we cannot hope to recover the true position of the object from the projection data alone. In [2], we accepted these ambiguities as inherent to the problem and defined equivalence classes of view angles and projection shifts. We take a different approach in this paper, the motivation and description of which are presented in Section III.

While the analysis in [2] was performed on noiseless projection data, in this paper, we will study the stability of the relevant problems when the projections are perturbed. We will consider two different perturbation models. The first is the fairly standard assumption in which each projection is corrupted by an additive Gaussian white noise process with power spectral density N_0

$$\hat{g}(s, i) = g(s, i) + n(s, i). \quad (2)$$

[1]We have restricted our study to real objects, but the methods and results in this paper extend in a straightforward way to complex valued objects.

We assume that the noise processes in different projections are uncorrelated. Such a model is very good for MRI, and plausible for X-ray tomography with high incidence counts. However, the analysis and algorithms in this paper apply to more general noise models, because they are only based on the assumption of Gaussian distributed estimates of the *moments* of the projections. The Gaussian model leads directly to Gaussian distributed moment estimates, but by the central limit theorem, it is also the asymptotic distribution for any other noise with bounded third moment for any system with discrete projections, as the number of samples per projection grows without bound. Because our analysis will operate on the assumption of a Gaussian distribution of the moments only, more general noise models for the projections can still be accommodated by this framework.

The second perturbation model we assume is a deterministic model, in which the noise signal $n(s, i)$ is constrained to have norm $\int n^2(s, i)\, ds \leq \delta$ for δ small. The two noise models are complementary. The Gaussian model leads to perturbations with arbitrarily large norm with nonzero probability, while the deterministic model makes no statistical assumptions about the noise signal, but requires that the overall perturbations be sufficiently small. We will rely on the results of [10] relating the two forms of stability.

III. Main Theoretical Results

In this section, we state our primary results on the stability of the ARP and SHARP. Although our main theorems will include statements regarding uniqueness of the solution, this subject has been treated in [2], and is included only for completeness.

A. Moment Formulation

Our analysis the ARP and SHARP is based on a moment characterization of the range space of the Radon Transform, known as the Helgasson-Ludwig (HL) consistency conditions. Let geometric moments of the object $f \in L_2(\mathbb{B}_2)$ being imaged be defined as

$$m_{i,k} = \iint_{\mathbb{B}_2} x^i y^k f(x, y)\, dx\, dy \qquad i \geq 0, k \geq 0 \quad (3)$$

and denote object moments of order d as the set of all $m_{i,k}$ such that $i + k = d$. Also, define

$$\mu_k(i) = \int_{\mathbb{B}} s^k g(s, i)\, ds \qquad i \in I, k \geq 0$$

the moments of the sinogram in $\{L_2(\mathbb{B})\}^P$. Then the fundamental result upon which our results are based is the HL condition, which relates the object moments $m_{i,k}$ to the projection moments $\mu_k(i)$ and view angles θ_i through trigonometric polynomials parameterized by the object moments.

The formal statement of the HL condition can be found in [9]. We will use the following version of the HL condition which is more convenient for our purposes.

Theorem 1: (HL Condition) If $g = \mathcal{R}_\theta f$ for some $\boldsymbol{\theta} \in \Omega^P$, $f \in L_2(\mathbb{B}_2)$, then for $d \geq 0, i \in I$

$$\mu_d(i) = \mathcal{Q}_d(\theta_i; \boldsymbol{m}) \quad (4)$$

where $\mathcal{Q}_d(\theta;\boldsymbol{m})$ are the HL trigonometric polynomials defined as

$$\mathcal{Q}_d(\theta;\boldsymbol{m}) = \sum_{r=0}^{d} \binom{d}{r} m_{r,\,d-r} \cos^r(\theta)\sin^{d-r}(\theta), \quad d \in D. \tag{5}$$

Throughout this section, we let D denote a fixed set of moment orders of the form $D = \{0, 1, \cdots, \Delta\}$. Then we denote by $\boldsymbol{m}$ the set of object moments of order $d \in D$, and

$$\eta(\Delta) \triangleq |\boldsymbol{m}| = \frac{(\Delta+1)(\Delta+2)}{2}.$$

We have suppressed the dependence of $\boldsymbol{m}$ on D to simplify the notation. We apply the HL condition to the ARP by first fixing D, and then seeking $\hat{\boldsymbol{\theta}}, \hat{\boldsymbol{m}}$ that satisfy

$$\mathcal{Q}_d(\hat{\theta}_i;\hat{\boldsymbol{m}}) - \mu_d(i) = 0 \qquad d \in D, i \in I. \tag{6}$$

Thus, we propose to determine the view angles θ by finding a set of object moments $\hat{\boldsymbol{m}}$ and view angles $\hat{\boldsymbol{\theta}}$ that produce projection moments that match $\mu_d(i)$ for $d \in D$. In [2], we referred to (6) as "data matching," for obvious reasons. Note that (6) is a system of nonlinear equations in $\hat{\boldsymbol{\theta}}$ and $\hat{\boldsymbol{m}}$, and that by Theorem 1, $(\hat{\boldsymbol{\theta}}, \hat{\boldsymbol{m}}) = (\boldsymbol{\theta}, \boldsymbol{m})$ is a solution to this system of equations.

B. Generic Subsets

Our study of uniqueness and stability for the ARP and SHARP builds upon our study of uniqueness in [2]. As a result, we need to discuss sets of objects in a measure-theoretic sense. In [2], we defined a *D-generic set* as a subset of $L_2(\mathbb{B}_2)$ with certain properties. We first extend that definition to the notion of a *D-generic subset* of a Lebesgue measurable set of objects $\Gamma \subset L_2(\mathbb{B}_2)$. For two sets A, B, let $A\backslash B$ denote the set difference of A and B.

Definition 3: (D-generic subset). For a given set of objects Γ, a subset S of Γ is a D-generic subset if the sets

$$C = \{D\text{-indexed moments of objects in } \Gamma\}$$
$$B = \{D\text{-indexed moments of objects in } \Gamma\backslash S\}$$

are such that B is a nowhere dense set of Lebesgue measure zero in C.

It follows that a D-generic subset of $L_2(\mathbb{B}_2)$, in the sense of Definition 3, is a D-generic set, in the sense of [2]. Let us now consider some properties fo D-generic subsets. If a property A holds for a D-generic subset of Γ, then it holds with probability one for objects whose D-indexed moments are drawn at random from an absolutely continuous probability distribution on Γ. Also, if a subset is D-generic, then we are guaranteed some measure of "robustness" with respect to membership in the subset. Because the set B of Definition 3 is a nowhere dense set of measure zero in C, it's complement has a nonempty interior. Thus, given an object f that belongs to the interior of a D-generic subset S, we can perturb that object and it will still belong to S, provided the perturbations in its D-indexed moments are sufficiently small. Finally, if a property A holds for a D-generic subset of Γ, then it also holds for "almost all objects in Γ," i.e., the statement that A is true for a D-generic subset of Γ is *stronger* than the statement that A is true for "almost all objects in Γ" (in the sense of Lebesgue measure on Γ [12]).[2] For future reference, we provide the following lemma about the intersection of D-generic subsets. The proof follows from Definition 3, and the fact that a finite union of nowhere dense sets of zero measure is also nowhere dense and of zero measure.

Lemma 1: If S_1 and S_2 are D-generic subsets of Γ, then so is $S_1 \cap S_2$.

C. Fixing Nonuniqueness

In [2], we actually demonstrated that there were infinitely many $(\hat{\boldsymbol{\theta}}, \hat{\boldsymbol{m}}) \neq (\boldsymbol{\theta}, \boldsymbol{m})$ that satisfied the "data matching" conditions of the ARP. These alternate solutions emerge from the fact that the (unknown) object can be rotated through some (unknown) angle α or reflected about the origin, without affecting the observed projection data. Although this uncertainty could be handled within the context of the uniqueness theory by defining equivalence classes, when studying stability we prefer to consider problems with a unique solution (or at least finitely many solutions). Thus, we inject some *a priori* information about $\boldsymbol{m}$ that fixes a unique solution to the data matching conditions (a particular element of the equivalence class of solutions considered in [2]). In particular, for the ARP, we assume that $D > 1$ and that $\boldsymbol{m}$ belongs to the following set:

$$W_1 = \{\boldsymbol{m}\text{: } m_{0,1} = 0, m_{1,0} \geq 0\}. \tag{7}$$

We also define the set of objects [i.e., elements of $L_2(\mathbb{B}_2)$] with moments in W_1

$$F_1 = \{f \in L_2(\mathbb{B}_2)\text{: } \boldsymbol{m} \in W_1\}. \tag{8}$$

To explain (7), consider the rotation of an object f through an angle α

$$f'(x,y) = f(x\cos\alpha - y\sin\alpha, x\sin\alpha + y\cos\alpha).$$

Then the moments $m'_{0,1}$ and $m'_{1,0}$ of f' are related to the moments $m_{0,1}$ and $m_{1,0}$ of f by

$$\begin{bmatrix} m'_{1,0} \\ m'_{0,1} \end{bmatrix} = \begin{bmatrix} \cos\alpha & \sin\alpha \\ -\sin\alpha & \cos\alpha \end{bmatrix} \begin{bmatrix} m_{1,0} \\ m_{0,1} \end{bmatrix}.$$

Thus, there always exists a rotation α of any object f for which $m'_{1,0} = 0$.

Next, consider a reflection of the object about the origin, i.e., $f'(x,y) = f(-x,-y)$. It is trivial to show that $m'_{0,1} = -m_{0,1}$ and $m'_{1,0} = -m_{1,0}$. Thus, by rotating f through some angle α and possibly reflecting it about the origin, we can map $\boldsymbol{m}$ into W_1. In the terminology of [2], we can take any object $f \in L_2(\mathbb{B}_2)$, and apply an orthogonal transformation to it so that lies in F_1. Furthermore, the original object and the transformed object cannot be distinguished on the basis of the projection data alone. Therefore, for the ARP, we restrict our attention, without

[2]In particular, using the sets in Definition 3, if B is a nowhere dense set of zero measure in C, then $\Gamma\backslash S$ must be a nowhere dense set of zero measure in Γ (however, the converse is not necessarily true). Thus, if a property A is true for a D-generic subset S of Γ, then it can only fail on $\Gamma\backslash S$, which must have measure zero, and thus A is true for almost all objects.

loss of generality, to objects in F_1. For objects in this set, we have the following result on uniqueness, the proof of which is based directly on the results of [2], and is included in Appendix A.

Theorem 2: (Uniqueness of the ARP). Suppose the projection data are acquired at P π-distinct view angles $\boldsymbol{\theta} = \{\theta_1, \theta_2, \cdots, \theta_P\}$, and suppose $\theta_i \notin \{(\pi/2), (-\pi/2)\}$ for any i [3]. Let S denote the set of objects in F_1 such that $\boldsymbol{\theta}$ is uniquely determined by the projection moments of order {0, 1, 2}. If $P > 8$, then S is a {0, 1, 2}-generic subset of F_1.

We fix the nonuniqueness of the SHARP in a similar way. In particular, we assume that $D > 2$, and define the following set:

$$W_2 = \{\boldsymbol{m}\colon m_{0,1} = m_{1,0} = 0, m_{1,1} = 0, m_{3,0} \geq 0\}. \quad (9)$$

We also define the set of objects [i.e., elements of $L_2(\mathbb{B}_2)$] with moments in W_2

$$F_2 = \{f \in L_2(\mathbb{B}_2)\colon \boldsymbol{m} \in W_2\}. \quad (10)$$

Using arguments similar to those just used, one can show that for the appropriate choice of a rigid body transformation, any object $f \in L_2(\mathbb{B}_2)$ can be transformed so that it lies in F_2, and furthermore, it is not possible to distinguish between the two by only using the projection data. The necessary transformation consists of

1) shifting the object so that its center of mass is at the origin;
2) rotating the object about the origin until $m_{1,1} = 0$;
3) reflecting the object about the origin (if needed) so that $m_{3,0} \geq 0$.

Therefore, for SHARP, we restrict our attention, without loss of generality, to objects in F_2. With this restriction, the SHARP has a unique solution.

Theorem 3: (Uniqueness of the SHARP). Suppose the projection data are acquired at P π-distinct view angles $\boldsymbol{\theta} = \{\theta_1, \theta_2, \cdots, \theta_P\}$. Let S denote the set of objects in F_2 such that $\boldsymbol{\theta}$, $\boldsymbol{\delta}$ are uniquely determined by the projection moments of order {0, 1, 2, 3}. If $P > 25$, then S is a {0, 1, 2, 3}-generic subset of F_2.

The proof is given in Appendix B.

D. Stability of Solutions to Nonlinear Least Squares Problems

To examine the stability of the ARP and SHARP in the presence of errors in the projection moments, we adopt a notion of stability that covers both the stochastic error formulation and the deterministic notion of stability simultaneously. To do so, we will use the results of [10], in which we discuss the stability of nonlinear least squares problems of the kind that arise in studying the SHARP and ARP. The generic estimation problem we consider in [10] is defined by the measurement equation

$$\boldsymbol{y} = \boldsymbol{F}(\boldsymbol{z}_0) + \boldsymbol{n} \quad (11)$$

[3]The odd-looking requirement on the view angles is a consequence of the fact that for every object, there are exactly two angles (called the unidentifiable angle set (UAS) in [2]) which cannot be uniquely identified from the {0, 1, 2} order projection moments. It so happens that for objects in F_1, these angles lie exactly at $\pm(\pi/2)$. The condition is an artifact of our treatment of uniqueness, and poses no problems in a practical setting, where considering more projection moments can uniquely resolve these angles. See [2], Section VII for more details.

where $\boldsymbol{F}\colon Z \to \mathbb{R}^l$ is a twice continuously differentiable map, which maps the vector of unknowns $\boldsymbol{z}_0 \in Z \subset \mathbb{R}^k$ into the observation $\boldsymbol{y} \in \mathbb{R}^l$, which is corrupted by additive noise $\boldsymbol{n}$. We assume that Z has a nonempty interior, denoted $\overset{\circ}{Z}$. We first state the two definitions of stability that we examine, keeping in line with the two noise models proposed in the previous section.

In a deterministic context, we are interested in the stability of least squares problem

$$\hat{\boldsymbol{z}}(\boldsymbol{y}) = \arg\min_{\boldsymbol{z} \in Z} \|\boldsymbol{y} - \boldsymbol{F}(\boldsymbol{z})\|^2. \quad (12)$$

We first define a strict global minimizer, the existence of which guarantees that (12) is a valid expression, in the sense that the set of minimizers is a single point.

Definition 4: (Strict Global Minimizer). A vector $\hat{\boldsymbol{z}} \in Z$ is a strict global minimizer of $\|\boldsymbol{y} - \boldsymbol{F}(\boldsymbol{z})\|^2$ with respect to $\boldsymbol{z}$ for fixed $\boldsymbol{z}_0$ and $\boldsymbol{n}$, if

$$\|\boldsymbol{y} - \boldsymbol{F}(\hat{\boldsymbol{z}})\|^2 < \|\boldsymbol{y} - \boldsymbol{F}(\boldsymbol{z}')\|^2 \quad \forall \boldsymbol{z}' \in Z, \boldsymbol{z}' \neq \hat{\boldsymbol{z}}$$

i.e., $\hat{\boldsymbol{z}}$ satisfies (12).

We can then define a deterministic sense of stability for a nonlinear least squares (NLS) problem at a point $\boldsymbol{z}_0$ in terms of the behavior of the strict global minimizer with respect to changes in $\boldsymbol{n}$. We will restrict ourselves to situations where $\boldsymbol{z}_0$, the noise-free solution, lies in $\overset{\circ}{Z}$ for the sake of simplicity. In the following definition, we use $B_\varepsilon(\mathbf{0})$ to denote the closed ball of radius ε centered at $\mathbf{0}$, i.e., $B_\varepsilon(\mathbf{0}) = \{\boldsymbol{n}\colon \|\boldsymbol{n}\| \leq \mathbf{0}\}$.

Definition 5: (Deterministic Stability). The NLS problem of (12) is said to be deterministically stable at $\boldsymbol{z} = \boldsymbol{z}_0$ if $\hat{\boldsymbol{z}} = \boldsymbol{z}_0$ is a strict global minimizer of $\|F(\boldsymbol{z}_0) - F(\boldsymbol{z})\|$, and if there exists $\varepsilon > 0$ and a continuously differentiable function $\phi\colon B_\varepsilon(\mathbf{0}) \to Z$ such that $\phi(\boldsymbol{n})$ is a strict global minimizer of $\|\boldsymbol{F}(\boldsymbol{z}_0) + \boldsymbol{n} - \boldsymbol{F}(\boldsymbol{z})\|$ for all $\boldsymbol{n} \in B_\varepsilon(\mathbf{0})$.

In other words, problem (12) is stable at $\boldsymbol{z} = \boldsymbol{z}_0$ if it has a unique solution for any sufficiently small noise, $\|\boldsymbol{n}\| < \varepsilon$, and this solution depends in a continuous and differentiable way on the noise. This is a strong form of stability for an inverse problem. It implies, among other things, Lipschitz continuity of the solution to (12) with respect to sufficiently small noise perturbations $\boldsymbol{n}$.

In a stochastic framework, we examine bounds on the covariance of unbiased estimators of $\boldsymbol{z}_0$ given $\boldsymbol{y}$ via the Cramér-Rao bound (CRB). To define the stochastic counterpart to stability, we must first recall the famous information inequality, and its principal component, the Fisher Information Matrix (FIM). Let $p(\boldsymbol{y}; \boldsymbol{z})$ denote the probability density function (pdf) of the observations $\boldsymbol{y}$ for a given value of the parameter $\boldsymbol{z}$. Then the FIM, assuming it exists, is defined as

$$\tilde{\boldsymbol{I}}_{\boldsymbol{z}_0} = -\mathrm{E}_{\boldsymbol{z}=\boldsymbol{z}_0}\{(\nabla_{\boldsymbol{z}} \log p(\boldsymbol{y}; \boldsymbol{z}))\,(\nabla_{\boldsymbol{z}} \log p(\boldsymbol{y}; \boldsymbol{z}))^T\} \quad (13)$$

where the expectation, as indicated by the notation, is taken with $\boldsymbol{z} = \boldsymbol{z}_0$ (the tilde distinguishes the FIM from an identity matrix). This matrix is always positive semidefinite. When it is positive definite, then the covariance of any unbiased estimator $\hat{\boldsymbol{z}}(\boldsymbol{y})$ of $\boldsymbol{z}_0$ is bounded below by

$$\mathrm{cov}\{\hat{\boldsymbol{z}}(\boldsymbol{y})\} \geq \boldsymbol{J}_{\boldsymbol{z}_0} \triangleq \tilde{\boldsymbol{I}}_{\boldsymbol{z}_0}^{-1}. \quad (14)$$

The stochastic counterpart to stability is defined in terms of (14).

Definition 6: (Stochastic Stability). The nonlinear parameter estimation problem defined by (11) is stochastically stable at $\boldsymbol{z}_0 \in \overset{\circ}{Z}$ if $\tilde{\boldsymbol{I}}_{\boldsymbol{z}_0}$ is positive definite, i.e., the lower bound of (14) is finite.

Further details on the CRB and the FIM can be found in [11].

A simple univariate example can demonstrate instability in both the deterministic and stochastic senses. Consider the problem of estimating the parameter z from the measurement $y = z^3 + n$. The least squares solution in this case is simply $\hat{z}(n) = y^{1/3} = (z_0 + n)^{1/3}$. If $z_0 = 0$, then the least squares problem is *not* stable at z_0 in the deterministic sense, as $\hat{z}(n)$ is not differentiable at $n = 0$. This particular example with a Gaussian distribution for the noise, i.e., $n \sim \mathcal{N}(0, \sigma^2)$ is not stable at $z_0 = 0$ in the stochastic sense either. The CRB for this noise distribution is $\sigma^2/(36z_0^4)$, which is not finite for $z_0 = 0$. Thus, it is impossible to construct an unbiased estimator for z that has finite variance when $z_0 = 0$. An important feature of this particular parameter estimation problem is that the underlying noiseless problem admits a unique solution, because in the absence of noise (i.e., $n = 0$), there is a unique $\hat{z}$ that satisfies $y = \hat{z}^3$. Thus, knowing that the problem admits a unique solution in the noiseless case is clearly not sufficient to establish stability of the problem in the presence of noise. Furthermore, for this example, the problem is stable (in both senses) for all other choices of z_0. A situation analogous to this occurs for the ARP and SHARP, in which the parameter values for which the problems are unstable are neither obvious nor accessible by systematic numerical exploration.

The previous example suggested a connection between the two senses of stability. We explore this connection in greater detail in [10]. The key result from that work, however, is the following theorem, which relates the linearization of the problem at $\boldsymbol{z}_0$ to *both* senses of stability.

Theorem 4: (Basu and Bresler [10]). Let $\boldsymbol{F}$: $Z \rightarrow Y$ be a continuous map, where $Z \subset \mathbb{R}^k$, $Y \subset \mathbb{R}^l$. Suppose that $\boldsymbol{F}$ is twice continuously differentiable in an open neighborhood of $\boldsymbol{z}_0 \in \overset{\circ}{Z}$, and $\boldsymbol{z}_0$ is identifiable (i.e., $\boldsymbol{F}(\boldsymbol{z}') = \boldsymbol{F}(\boldsymbol{z}_0) \Longrightarrow \boldsymbol{z}' = \boldsymbol{z}_0$). Then, the following are equivalent:

1) gradient matrix of $\boldsymbol{F}$, defined by $[\boldsymbol{G}(\boldsymbol{z}_0)]_{i,j} = (\partial \boldsymbol{F}_i(\boldsymbol{z})/\partial z_j)|_{\boldsymbol{z}=\boldsymbol{z}_0}$, is full column rank;
2) nonlinear least squares problem is stable in the deterministic sense at $\boldsymbol{z}_0$;
3) nonlinear parameter estimation problem is stable in the stochastic sense at $\boldsymbol{z}_0$ for Gaussian noise.

Thus, we will concern ourselves with establishing that the appropriate gradient matrices for the ARP and SHARP are full column rank. An additional consequence of Theorem 4 is that we can simply refer to the problem as "stable at $\boldsymbol{z}_0$," because if we demonstrate that the gradient matrix is full-column rank, then the problem is stable at $\boldsymbol{z}_0$ under either noise model discussed in the previous section. Finally, the gradient matrix $\boldsymbol{G}$ can also be used to calculate the FIM, using the following well-known expression for the FIM for problems of the form (11) where $\boldsymbol{n} \sim \mathcal{N}(\boldsymbol{0}, \sigma^2 \boldsymbol{I})$:

$$\tilde{\boldsymbol{I}}_{\boldsymbol{z}_0} = \frac{1}{\sigma^2} \boldsymbol{G}(\boldsymbol{z}_0)^T \boldsymbol{G}(\boldsymbol{z}_0). \tag{15}$$

E. Stability Theorems

We can now state our main result on the stability of the ARP.

Theorem 5: (Stability of the ARP). Suppose the projection data are acquired at P π-distinct view angles $\boldsymbol{\theta} = \{\theta_1, \theta_2, \cdots, \theta_P\}$, and suppose that $\theta_i \notin \{(\pi/2), -(\pi/2)\}$. Let S denote the set of objects in F_1 (defined by (8)) for which

1) the view angles $\boldsymbol{\theta}$ are uniquely determined by the projection moments of order $\{0, 1, 2\}$;
2) the ARP is stable.

If $P > 8$, then S is a $\{0, 1, 2\}$-generic subset of F_1. Hence, for $P > 8$, and a $\{0, 1, 2\}$-generic subset of objects from F_1, the ARP has a unique solution, and is stable.

In view of the previous discussion of D-generic, we obtain the following (weaker) corollary.

Corollary 1: Suppose $\theta_1, \cdots, \theta_P$ are π-distinct. If $P > 8$, then the ARP has a unique solution and is stable for almost all objects in F_1.

A similar result (and interpretation) also holds for the SHARP.

Theorem 6: (Stability of SHARP). Suppose the projection data are acquired at P π-distinct view angles $\boldsymbol{\theta} = \{\theta_1, \theta_2, \cdots, \theta_P\}$ at shifts $\boldsymbol{\delta} = \{\delta_1, \delta_2, \cdots, \delta_P\}$. Let S denote the set of objects in F_2 (defined by (10)) for which

1) the view angles $\boldsymbol{\theta}$ and shifts $\boldsymbol{\delta}$ are uniquely determined by the projection moments of order $\{0, 1, 2, 3\}$;
2) the SHARP is stable.

If $P > 24$, then S is $\{0, 1, 2, 3\}$-generic subset of F_2. Hence, for $P > 24$, and a $\{0, 1, 2, 3\}$-generic subset of objects from F_2, the SHARP has a unique solution and is stable.

Corollary 2: Suppose $\theta_1, \cdots, \theta_P$ are π-distinct. If $P > 24$, then the SHARP has a unique solution and is stable for almost all objects in F_2.

IV. Stability of the ARP and SHARP

With Theorem 4 from the previous section, we can now turn to the task of demonstrating stability of the ARP and SHARP, i.e., proving Theorems 5 and 6. To do so, we will analyze the structure of the gradient matricesfor both problems, and establish conditions under which the matrix is full column rank. These conditions will then be used to prove Theorems 5 and 6. Before examining stability, we will reformulate the measurement equations in terms of Legendre moments so as to deal with statistically independent moments, and develop a matrix-function description of the problems (so as to apply Theorem 4).

A. Legendre Moments Reformulation

Under the Gaussian noise model (2), the geometric projection moments that we have been using so far will be correlated. This is an undesirable property in the subsequent analysis, so we modify the moments so as to decorrelate them. Before doing so, we note that the HL condition can be trivially generalized to the following.

Corollary 3: Let $p_d(s)$ be a polynomial of odd (even) degree d in s with strictly odd (even) powers of s, and suppose $f \in L_2(\mathbb{B}_2)$. Then if $g = \mathcal{R}_\theta f$ for some $\boldsymbol{\theta} \in \Omega^P$

$$\int_{\mathbb{B}} p_d(s) g(s,i)\, ds = \sum_{\substack{k \text{ odd (even)} \\ 0 \le k \le d}} a_{d,k} \cos(k\theta_i) + b_{d,k} \sin(k\theta_i) \quad (16)$$

for $i \in I$, $a_{d,k}, b_{d,k} \in \mathbb{R}$ with $a_{d,0} = b_{d,0}$.

Furthermore, $a_{d,k}$ and $b_{d,k}$ are linear combinations of $\{m_{r,k-r}\}_{r=0}^{k}$. Note that the coefficients $a_{d,k}$, $b_{d,k}$ in Corollary 3 can be regarded as "generalized object moments of order k," i.e., inner products of the object with a bivariate polynomial of total order k.

We then choose the $p_d(s)$ polynomials to be normalized Legendre polynomials $P_d(s)$, defined as [13]

$$P_d(s) = \frac{\sqrt{d+\frac{1}{2}}}{2^d d!} \frac{\partial^d}{\partial s^d} (s^2-1)^d \qquad s \in [-1,1] \quad (17)$$

which form an orthonormal set of polynomials under the unity weight on $\mathbb{B}$, i.e., $\int_{\mathbb{B}} P_k(s) P_j(s)\, ds = \delta(k-j)$, and which also satisfy the remaining requirements of Corollary 3 [13]. The resulting Legendre moments of the noisy projections, defined by

$$\hat{\omega}_d(i) = \int_{\mathbb{B}} P_d(s) \hat{g}(s,i)\, ds \quad (18)$$

can then be shown to be Gaussian random variables that are independent with respect to both i and d, with variance N_0, and means equal to the noiseless Legendre moments

$$\mathrm{E}\{\hat{\omega}_d(i)\} = \omega_d(i) \triangleq \int_{\mathbb{B}} P_d(s) g(s,i)\, ds. \quad (19)$$

For the purposes of bound calculations and algorithm development, we express Corollary 3 in matrix form. Note that for any d, there are exactly $d+1$ real coefficients in the right hand side of (16). We "pack" these coefficients in the following manner into a vector $\boldsymbol{x}_d \in \mathbb{R}^{d+1}$

$$\boldsymbol{x}_d = \begin{cases} a_{0,0} & d = 0 \\ [a_{d,0}, a_{d,2}, b_{d,2}, a_{d,4}, b_{d,4}, \cdots, a_{d,d}, b_{d,d}]^T & d \text{ even}, \\ [a_{d,1}, b_{d,1}, a_{d,3}, b_{d,3}, \cdots, a_{d,d}, b_{d,d}]^T & d \text{ odd}. \end{cases} \quad (20)$$

Next, let $\boldsymbol{v}_d$: $\Omega \to \mathbb{R}^{d+1}$ be the following vector valued function of θ

$$\boldsymbol{v}_d(\theta) = \left[\frac{1}{\sqrt{2}}, \cos(2\theta), \sin(2\theta), \cos(4\theta), \sin(4\theta), \cdots, \cos(d\theta), \sin(d\theta) \right]^T \quad (21)$$

if d is even

$$\boldsymbol{v}_d(\theta) = [\cos(\theta), \sin(\theta), \cos(3\theta), \sin(3\theta), \cdots, \cos(d\theta), \sin(d\theta)]^T$$

if d is odd, and $\boldsymbol{v}_0(\theta) = (1/\sqrt{2})$. Then (16) and (19) yield

$$\omega_d(i) = \boldsymbol{v}_d^T(\theta_i) \boldsymbol{x}_d. \quad (22)$$

To combine the moment relations for different orders and view angles, let $\boldsymbol{y}_i \in \mathbb{R}^{\Delta+1}$ denote the observation vector with the Legendre moments of projection i in consecutive order

$$\boldsymbol{y}_i = [\hat{\omega}_0(i), \hat{\omega}_1(i), \cdots, \hat{\omega}_\Delta(i)]^T. \quad (23)$$

Define the vector $\boldsymbol{x} = [x_0, \boldsymbol{x}_1^T, \cdots, \boldsymbol{x}_\Delta^T]^T \in \mathbb{R}^{\eta(\Delta)}$ of "generalized" object moments, i.e., inner products of the object f with polynomials. As we discussed in Section III-C, unique recovery of the view angles required that we restrict f to the set F_1. Now, using (5) and (16)–(19), it follows that $a_{1,1} = m_{0,1}$, and $b_{1,1} = m_{1,0}$. Hence, for $f \in F_1$, $(\boldsymbol{x}_1)_1 = 0$, and

$$\boldsymbol{x} = \boldsymbol{E}_1 \overline{\boldsymbol{x}} \quad (24)$$

where $\overline{\boldsymbol{x}} \in \mathbb{R}^{\eta(\Delta)-1}$, and $\boldsymbol{E}_1$ is the matrix obtained by deleting the second column of the $\eta(\Delta) \times \eta(\Delta)$ identity matrix. As for the constraint $m_{1,0} \ge 0$, implied by $f \in F_1$, (which reduces to $(\overline{\boldsymbol{x}})_2 \ge 0$), we will see shortly that it has no bearing on the questions of stability.

Next, we define the matrix function $\boldsymbol{S}$: $\Omega \to \mathbb{R}^{\Delta \times \eta(\Delta)}$ of θ as

$$\boldsymbol{S}(\theta) = \text{blockdiag}(v_0(\theta), \boldsymbol{v}_1^T(\theta), \cdots, \boldsymbol{v}_\Delta^T(\theta)). \quad (25)$$

It then follows from the stated noise model and (22)–(24) that the observation model for all projections $\boldsymbol{y} = [\boldsymbol{y}_1^T, \cdots, \boldsymbol{y}_P^T]^T$ of $f \in F_1$ can be written as

$$\boldsymbol{y} = \boldsymbol{\Xi}(\boldsymbol{\theta}) \overline{\boldsymbol{x}} + \boldsymbol{n}, \boldsymbol{\theta} \in \Omega^P, (\overline{\boldsymbol{x}})_2 \ge 0 \quad (26)$$

where $\boldsymbol{\Xi}$: $\Omega^P \to \mathbb{R}^{(P\Delta) \times (\eta(\Delta)-1)}$ is defined

$$\boldsymbol{\Xi}(\boldsymbol{\theta}) = \begin{bmatrix} \boldsymbol{S}(\theta_1) \\ \boldsymbol{S}(\theta_2) \\ \vdots \\ \boldsymbol{S}(\theta_P) \end{bmatrix} \boldsymbol{E}_1 \quad (27)$$

and $\boldsymbol{n} \sim \mathcal{N}(0, N_0 I)$.

With these definitions, we will exclusively consider the estimation of $(\boldsymbol{\theta}, \overline{\boldsymbol{x}})$ from the data $\boldsymbol{y}$, and use (26) as the measurement equation in our analysis.

B. ARP Stability

We now turn to analyzing the stability of the estimation problem defined by the measurement equation (26). Our vector $\boldsymbol{z}$ of unknown parameters is given by

$$[\boldsymbol{\theta}^T, \overline{\boldsymbol{x}}^T]^T \quad (28)$$

and our NLS problem is defined by (12) with $\boldsymbol{F}([\boldsymbol{\theta}^T, \overline{\boldsymbol{x}}^T]^T)$ defined by the first term on the right hand side of (26). The constraint set Z is also defined by (26) as

$$Z = \Omega^P \times \{\overline{\boldsymbol{x}}\text{: } (\overline{\boldsymbol{x}})_2 \ge 0\}. \quad (29)$$

Using the periodicity of $\boldsymbol{\Xi}(\boldsymbol{\theta})$ with respect to θ_i, it is simple to show that

$$\overset{\circ}{Z} = \Omega^P \times \{\overline{\boldsymbol{x}}\text{: } (\overline{\boldsymbol{x}})_2 > 0\}. \quad (30)$$

By Theorem 4, it follows that for $\boldsymbol{z}_0 \in \overset{\circ}{Z}$, stability of the ARP for $\boldsymbol{z}_0$ can be determined by studying the column rank of the appropriate matrix.

For the measurement model (26), the gradient matrix has the following structure:

$$\boldsymbol{G}(\boldsymbol{\theta}, \overline{\boldsymbol{x}}) = [\boldsymbol{G}_1(\boldsymbol{\theta}, \overline{\boldsymbol{x}}) | \boldsymbol{\Xi}(\boldsymbol{\theta})] \quad (31)$$

where $\boldsymbol{G}_1(\boldsymbol{\theta},\overline{\boldsymbol{x}}) \in \mathbb{R}^{(P\cdot\eta(\Delta)-1)\times P}$ is defined by

$$\boldsymbol{G}_1(\boldsymbol{\theta},\overline{\boldsymbol{x}}) = \begin{bmatrix} \dot{\boldsymbol{S}}(\theta_1)\boldsymbol{E}_1\overline{\boldsymbol{x}} & \boldsymbol{0} & \cdots & \boldsymbol{0} \\ \boldsymbol{0} & \dot{\boldsymbol{S}}(\theta_2)\boldsymbol{E}_1\overline{\boldsymbol{x}} & \ddots & \vdots \\ \vdots & \ddots & \ddots & \boldsymbol{0} \\ \boldsymbol{0} & \cdots & \boldsymbol{0} & \dot{\boldsymbol{S}}(\theta_P)\boldsymbol{E}_1\overline{\boldsymbol{x}} \end{bmatrix}$$

and $\dot{\boldsymbol{S}}(\theta_0) \triangleq ((\partial/\partial\theta)\boldsymbol{S})(\theta_0)$ is the componentwise derivative of $\boldsymbol{S}(\theta)$ with respect to the view angle. From this expression, (15), and simple matrix identities, we can write the CRB for the angle components $\boldsymbol{\theta}$ of $\boldsymbol{z}$ as

$$\boldsymbol{J}_{\boldsymbol{\theta}\boldsymbol{\theta}} = N_0(N_0\tilde{\boldsymbol{I}}_{\boldsymbol{\theta}\boldsymbol{\theta}} - \boldsymbol{G}_1^T\boldsymbol{\Xi}(\boldsymbol{\theta})(\boldsymbol{\Xi}(\boldsymbol{\theta})^T \cdot \boldsymbol{\Xi}(\boldsymbol{\theta}))^{-1}\boldsymbol{\Xi}(\boldsymbol{\theta})^T\boldsymbol{G}_1)^{-1} \tag{32}$$

where $\tilde{\boldsymbol{I}}_{\boldsymbol{\theta}\boldsymbol{\theta}} = (1/N_0)\boldsymbol{G}_1^T\boldsymbol{G}_1$ is the block of the FIM corresponding to the angular components.

The following theorem captures conditions for the gradient matrix to have full rank.

Theorem 7: Suppose that $\Delta = 2$, $P > 5$, and that the θ_i are π-distinct and fixed *a priori*. Suppose that $(\overline{\boldsymbol{x}})_1, (\overline{\boldsymbol{x}})_2, (\overline{\boldsymbol{x}})_5 \neq 0$. Then $\boldsymbol{G}(\boldsymbol{\theta},\overline{\boldsymbol{x}})$ defined by (31) is full rank.

The proof is essentially algebraic, and can be found in [14].

With the aid of Theorem 7, we can prove Theorem 5 quite easily.

Proof: [Theorem 5] Let

$$S_1 \triangleq \{\text{objects in } F_1 \text{ such that the ARP has a unique solution}\}$$

and

$$S_2 \triangleq \{\text{objects in } F_1 \text{ such that } \boldsymbol{G}(\boldsymbol{\theta},\overline{\boldsymbol{x}}) \text{ has full column rank}\}.$$

By Theorems 2 and 7, it follows that S_1 and S_2 respectively are $\{1, 2\}$-generic subsets of F_1. Let

$$S' = S_1 \cap S_2 \cap \{\text{objects in } F_1 \text{ s.t. } (\overline{\boldsymbol{x}})_2 > 0\}.$$

With Z defined by (29), it follows that for any object in S' and any set of view angles $\boldsymbol{\theta}$ with $\theta_i \notin \{-(\pi/2), (\pi/2)\}$, $[\boldsymbol{\theta}^T, \overline{\boldsymbol{x}}^T]^T \in \overset{\circ}{Z}$. By Theorem 4, it follows that the ARP is stable for this choice of $\boldsymbol{\theta}$ and object. By Lemma 1, S' is a $\{1, 2\}$-generic subset of F_1. Now, the set S defined in Theorem 5 must contain S', and therefore, it too is a $\{1, 2\}$-generic subset of F_1. ∎

C. SHARP Stability

For the SHARP, we observe a noisy version of the shifted sinogram

$$\hat{\tilde{g}}(s,i) = \tilde{g}(s,i) + n(s,i) = g(s-\delta_i,i) + n(s,i)$$

where the shifts δ_i are unknowns, along with the view angles θ_i. The dth Legendre moment of $\hat{\tilde{g}}$, denoted $\hat{\tilde{\omega}}_d(i)$, is defined by $\hat{\tilde{\omega}}_d(i) = \int P_d(s)\hat{\tilde{g}}(s,i)\,ds$ where $P_d(s)$ is defined in (17). We also denote $\tilde{\omega}_d(i) = \mathrm{E}\{\hat{\tilde{\omega}}_d(i)\}$.

There are several approaches to estimating the unknown δ_i's. The most general is to jointly estimate the shifts with the view angles and object moments. Treated as such, the shifts simply add an additional layer of complexity to the estimation problem. Another approach is object-specific, and involves the locating of "alignment cues" or point-like features that can be placed at the center of the reference frame. This approach suffers from a lack of generality, but effectively decouples the shift and angle estimation problems. In this paper, we develop results exclusively on the first approach.

To facilitate the calculation of a gradient matrix, we first relate the Legendre moments of the shifted projections to the geometric moments of the unshifted projections. Let the dth Legendre polynomial be written as

$$P_d(s) = \sum_{i\le d} a_{d,i}s^i.$$

For a fixed D, we then define the matrix function of $\delta \in \mathbb{R}$ as $\boldsymbol{T}$: $\mathbb{R} \to \mathbb{R}^{\Delta\times\Delta}$, with

$$(\boldsymbol{T}(\delta))_{k,l} = \begin{cases} \displaystyle\sum_{l\le j\le k} \binom{k}{l} a_{k,j}\delta^{j-l}, & k \ge l \\ 0, & \text{else.} \end{cases}$$

Then it is simple to show that

$$\begin{bmatrix} \tilde{\omega}_0(i) \\ \tilde{\omega}_1(i) \\ \vdots \\ \tilde{\omega}_\Delta(i) \end{bmatrix} = \boldsymbol{T}(\delta_i)\begin{bmatrix} \mu_0(i) \\ \mu_1(i) \\ \vdots \\ \mu_\Delta(i) \end{bmatrix}$$

and that $\boldsymbol{T}(\boldsymbol{\delta})$ is nonsingular for any δ because it is lower triangular with constant, nonzero diagonal entries. Also, by Corollary 3, we can define $\boldsymbol{x} \in \mathbb{R}^{\eta(\Delta)}$ such that

$$\begin{bmatrix} \mu_0(i) \\ \mu_1(i) \\ \vdots \\ \mu_\Delta(i) \end{bmatrix} = \boldsymbol{S}(\theta_i)\boldsymbol{x}.$$

Now, we incorporate the constraint set F_2 into the matrix formulation. By repeating the arguments used for the ARP, we find that for $f \in F_2$

$$\boldsymbol{x} = \boldsymbol{E}_2\overline{\boldsymbol{x}} \tag{33}$$

where $\overline{\boldsymbol{x}} \in \mathbb{R}^{\eta(\Delta)-3}$, and $\boldsymbol{E}_2$ is the matrix obtained by deleting columns 2, 3, 5 from the $\eta(\Delta)\times\eta(\Delta)$ identity matrix.

Defining $\tilde{\boldsymbol{y}} = [\tilde{\boldsymbol{y}}_1^T, \cdots, \tilde{\boldsymbol{y}}_P^T]^T$, and

$$\tilde{\boldsymbol{y}}_i = [\tilde{\omega}_0(i), \cdots, \tilde{\omega}_\Delta(i)]^T,$$

we can write, in a manner analogous to (26):

$$\tilde{\boldsymbol{y}} = \boldsymbol{\Xi}(\boldsymbol{\theta},\boldsymbol{\delta})\overline{\boldsymbol{x}} + \boldsymbol{n}, \quad \boldsymbol{\theta} \in \Omega^P, \boldsymbol{\delta} \in \mathbb{R}^P, (\overline{\boldsymbol{x}})_4 \ge 0, \tag{34}$$

where

$$\boldsymbol{\Xi}(\boldsymbol{\theta},\boldsymbol{\delta}) = \begin{bmatrix} \boldsymbol{T}(\delta_1)\boldsymbol{S}(\theta_1) \\ \boldsymbol{T}(\delta_2)\boldsymbol{S}(\theta_2) \\ \vdots \\ \boldsymbol{T}(\delta_P)\boldsymbol{S}(\theta_P) \end{bmatrix}\boldsymbol{E}_2.$$

For the SHARP, the unknown parameters lie in $\Omega^P \times \mathbb{R}^P \times \mathbb{R}^{\eta(\Delta)-3}$, and are defined by the vector

$$[\boldsymbol{\theta}^T, \boldsymbol{\delta}^T, \overline{\boldsymbol{x}}^T]^T \tag{35}$$

with the mapping $\boldsymbol{F}([\boldsymbol{\theta}^T, \boldsymbol{\delta}^T, \overline{\boldsymbol{x}}^T]^T)$ defined by (34) with $\boldsymbol{n} = 0$ and

$$Z = \Omega^P \times \mathbb{R}^P \times \{\overline{\boldsymbol{x}}\text{: } (\overline{\boldsymbol{x}})_4 \ge 0\}. \tag{36}$$

The gradient matrix of $\boldsymbol{F}$ with respect to the unknown parameters is then

$$\boldsymbol{G}(\boldsymbol{\theta},\boldsymbol{\delta},\overline{\boldsymbol{x}}) = [\boldsymbol{G}_1(\boldsymbol{\theta},\boldsymbol{\delta},\overline{\boldsymbol{x}})|\boldsymbol{G}_2(\boldsymbol{\theta},\boldsymbol{\delta},\overline{\boldsymbol{x}})|\boldsymbol{\Xi}(\boldsymbol{\theta},\boldsymbol{\delta})] \quad (37)$$

with

$$\boldsymbol{G}_1 = \begin{bmatrix} \dot{\boldsymbol{T}}(\delta_1)\boldsymbol{S}(\theta_1)\boldsymbol{E}_2\overline{\boldsymbol{x}} & & 0 \\ & \ddots & \\ 0 & & \dot{\boldsymbol{T}}(\delta_P)\boldsymbol{S}(\theta_P)\boldsymbol{E}_2\overline{\boldsymbol{x}} \end{bmatrix},$$

$$\boldsymbol{G}_2 = \begin{bmatrix} \boldsymbol{T}(\delta_1)\dot{\boldsymbol{S}}(\theta_1)\boldsymbol{E}_2\overline{\boldsymbol{x}} & & 0 \\ & \ddots & \\ 0 & & \boldsymbol{T}(\delta_P)\dot{\boldsymbol{S}}(\theta_P)\boldsymbol{E}_2\overline{\boldsymbol{x}} \end{bmatrix}$$

and the matrix function $\dot{\boldsymbol{T}}$ is defined as $\dot{\boldsymbol{T}}(\delta_0) = ((\partial/\partial\delta)\boldsymbol{T})(\delta_0)$.

Analogous to Theorem 7, there are some technical conditions that must be satisfied for the gradient matrix to be full rank.

Theorem 8: Suppose that $\Delta = 3$, $P > 9$, and that the θ_i are π-distinct and fixed *a priori*. Suppose further that $(\overline{\boldsymbol{x}})_1$, $(\overline{\boldsymbol{x}})_2$, $(\overline{\boldsymbol{x}})_3 \neq 0$, at least one of $(\overline{\boldsymbol{x}})_4$, $(\overline{\boldsymbol{x}})_5$, $(\overline{\boldsymbol{x}})_6$, $(\overline{\boldsymbol{x}})_7$ is nonzero, and either $(\overline{\boldsymbol{x}})_5 \neq 3(\overline{\boldsymbol{x}})_7$ or $(\overline{\boldsymbol{x}})_4 \neq -3(\overline{\boldsymbol{x}})_6$. Then $\boldsymbol{G}(\boldsymbol{\theta},\boldsymbol{\delta},\overline{\boldsymbol{x}})$ defined by (37) is full rank.

The proof can be found in [14]. With the aid of Theorem 8, we can prove Theorem 6 in a manner completely analogous to the proof of Theorem 5.

V. Additional Bounds

We next turn to deriving some additional performance bounds of interest for the ARP and SHARP. These bounds will help characterize performance numerically and provide benchmarks for evaluating the simulation results. They are not related to stability results for either problem, and are thus treated separately.

A. Useful Moment Orders

It is possible to determine *a priori* an upper bound on the maximum number of moments that are useful in solving the ARP and SHARP. In particular, the following theorem indicates the behavior of the MLE and CRB for the view angles in the ARP for moments of order $d \geq P-1$. We first define the maximum likelihood estimate of $\boldsymbol{\theta}$ as a function of Δ, which we obtain by maximizing the concentrated likelihood

$$\hat{\boldsymbol{\theta}}_{\mathrm{ML}}(\Delta) = \arg\max_{\boldsymbol{\theta}} \|\boldsymbol{P}_{\boldsymbol{\Xi}(\boldsymbol{\theta})}\boldsymbol{y}\|^2 \quad (38)$$

where $\boldsymbol{P}_{\boldsymbol{\Xi}(\boldsymbol{\theta})} = \boldsymbol{\Xi}(\boldsymbol{\Xi}^T\boldsymbol{\Xi})^{-1}\boldsymbol{\Xi}^T(\boldsymbol{\theta})$. We also define the CRB for estimating $\boldsymbol{\theta}$, by rewriting (32) as

$$\boldsymbol{J}_{\boldsymbol{\theta\theta}}(\Delta) = N_0(\boldsymbol{G}_1^T\boldsymbol{P}_{R(\boldsymbol{\Xi}(\boldsymbol{\theta}))^\perp}\boldsymbol{G}_1)^{-1}.$$

Theorem 9: For any object, and for any P projections with θ_i, $i \in I$ π-distinct, the following identities hold for all $\Delta \geq P-1$:

1) $\hat{\boldsymbol{\theta}}_{\mathrm{ML}}(\Delta) = \hat{\boldsymbol{\theta}}_{\mathrm{ML}}(P-2)$;
2) $\boldsymbol{J}_{\boldsymbol{\theta\theta}}(\Delta) = \boldsymbol{J}_{\boldsymbol{\theta\theta}}(P-2)$.

To prove this result, we introduce the following definitions. We define the matrix $\boldsymbol{A}_d(\boldsymbol{\theta}) \in \mathbb{R}^{P\times(d+1)}$ as

$$\boldsymbol{A}_d(\boldsymbol{\theta}) = [\boldsymbol{v}_d(\theta_1),\cdots,\boldsymbol{v}_d(\theta_P)]. \quad (39)$$

These matrices have a special property in that they are provably full row rank for $d \geq (P-1)$.

Lemma 2: If θ_i are π-distinct for all $i \in I$, and $d \geq (P-1)$, then $\boldsymbol{A}_d(\boldsymbol{\theta}) \in \mathbb{R}^{P\times(d+1)}$ defined by has full row rank.

Proof: By elementary column operations, $\boldsymbol{A}_n^T(\boldsymbol{\theta})$ can be transformed into

$$\begin{bmatrix} 1 & 1 & \cdots & 1 \\ e^{j\phi_1} & e^{j\phi_2} & \cdots & e^{j\phi_P} \\ \vdots & \vdots & \vdots & \vdots \\ e^{j\phi_1^n} & e^{j\phi_2^n} & \cdots & e^{j\phi_P^n} \end{bmatrix}$$

where $\phi_i = 2\theta_i$. This matrix has Vandermonde structure, and is full column rank provided the θ_i's are π-distinct. ■

Proof: [Theorem 9] It can easily be shown that

$$\boldsymbol{\Xi}(\boldsymbol{\theta}) = \boldsymbol{E}\begin{bmatrix} \boldsymbol{A}_0(\boldsymbol{\theta}) & 0 & \cdots & 0 \\ 0 & \boldsymbol{A}_1(\boldsymbol{\theta}) & \ddots & \vdots \\ \vdots & \ddots & \ddots & 0 \\ 0 & \cdots & 0 & \boldsymbol{A}_\Delta(\boldsymbol{\theta}) \end{bmatrix}\boldsymbol{E}_1$$

where $\boldsymbol{E}$ is a permutation matrix. Furthermore, it follows from $\boldsymbol{E}^T\boldsymbol{E} = \boldsymbol{I}$ that

$$\boldsymbol{P}_{R(\boldsymbol{\Xi}(\boldsymbol{\theta}))^\perp} = \boldsymbol{E}\begin{bmatrix} \boldsymbol{P}_{R(\boldsymbol{A}_0(\boldsymbol{\theta}))^\perp} & 0 & \cdots & 0 \\ 0 & \boldsymbol{P}_{R(\boldsymbol{A}_1(\boldsymbol{\theta}))^\perp} & \ddots & \vdots \\ \vdots & \ddots & \ddots & 0 \\ 0 & \cdots & 0 & \boldsymbol{P}_{R(\boldsymbol{A}_\Delta(\boldsymbol{\theta}))^\perp} \end{bmatrix}\boldsymbol{E}^T.$$

Now, by Lemma 2, it follows that $\boldsymbol{P}_{R(\boldsymbol{A}_d(\boldsymbol{\theta}))^\perp} = 0$ for $d \geq P-1$. Theorem 9 then follows in a straightforward manner from this observation. ■

A result similar to Theorem 9 holds for the SHARP. Let $[\hat{\boldsymbol{\theta}}_{\mathrm{ML}},\hat{\boldsymbol{\delta}}_{\mathrm{ML}}](\Delta)$ be the maximum likelihood estimate of $\boldsymbol{\theta}$, $\hat{\boldsymbol{\delta}}$ as a function of Δ, obtained in a similar manner to (38) by maximizing the concentrated likelihood. Also, define the CRB for joint estimation of $\boldsymbol{\theta}$, $\boldsymbol{\delta}$ as the following matrix valued function of Δ:

$$\boldsymbol{J}_{\mathrm{SHARP}}(\Delta) = \begin{bmatrix} \boldsymbol{J}_{\boldsymbol{\theta\theta}} & \boldsymbol{J}_{\boldsymbol{\theta\delta}} \\ \boldsymbol{J}_{\boldsymbol{\delta\theta}} & \boldsymbol{J}_{\boldsymbol{\delta\delta}} \end{bmatrix}.$$

We can then state the following theorem, omitting the proof, which is very similar to that of Theorem 9.

Theorem 10: For any object, and for any P projections with θ_i, $i \in I$ π-distinct, and $\delta_i \in \mathbb{R}$, the following identities hold for all $\Delta \geq P-1$:

1) $[\hat{\boldsymbol{\theta}}_{\mathrm{ML}},\hat{\boldsymbol{\delta}}_{\mathrm{ML}}](\Delta) = [\hat{\boldsymbol{\theta}}_{\mathrm{ML}},\hat{\boldsymbol{\delta}}_{\mathrm{ML}}](P-2)$;
2) $\boldsymbol{J}_{\mathrm{SHARP}}(\Delta) = \boldsymbol{J}_{\mathrm{SHARP}}(P-2)$.

The two theorems suggest that the first $P-2$ moments "contain all the useful information" in the projections, and are sufficient (in terms of the MLE and CRB) for estimation of the view angles and shifts. We will examine (numerically) how many moments are practically useful in the next section.

B. Known-Object Bounds

In this subsection, we develop CRB's for the case of *known* object moments. This bound serves two purposes. The primary purpose is to provide a lower bound on the results of the previous section for situations in which numerical difficulties preclude calculation of the general CRB. The second purpose is to present a basis of comparison between the case of a known object and an unknown object. Our goal will be to quantify the "loss" in

estimator performance that arises from not knowing the object being imaged. We will characterize this difference in the bounds in a later subsection.

Consider the case of moment-based estimates of the angles when the vector $\boldsymbol{x}$ of generalized object moments is known. This assumption is akin to assuming the object itself is known, but that only $\boldsymbol{x}$ is used in the estimation of $\boldsymbol{\theta}$. The gradient matrix for this problem is clearly $\boldsymbol{G}_1$ (with $\boldsymbol{x}$ fixed) of (31), from which the FIM and thus the Cramér-Rao bound is

$$\tilde{\boldsymbol{I}}_{\text{known}} = \frac{1}{N_0}\, \boldsymbol{G}_1^T(\boldsymbol{\theta})\boldsymbol{G}_1(\boldsymbol{\theta}), \qquad \boldsymbol{J}_{\text{known}} = \tilde{\boldsymbol{I}}_{\text{known}}^{-1}. \quad (40)$$

From (31), it is immediate that $\tilde{\boldsymbol{I}}_{\text{known}}$ is diagonal, implying that in the known object case the angle estimation problem decouples. Note that for stability, we require that $\dot{\boldsymbol{S}}(\theta_i)\boldsymbol{x} \neq 0$ for all $1 \leq i \leq P$, a condition that is easily satisfied, as discussed previously.

Besides providing a lower bound on the CRB's computed in the previous section for large P, we would expect the known object moment bounds to characterize the performance of methods as P grows without bound.[4] To see why, we can rewrite (32) for the case that the angles are equally spaced, in which case

$$\boldsymbol{J}_{\boldsymbol{\theta\theta}} = N_0 \left(N_0 \tilde{\boldsymbol{I}}_{\boldsymbol{\theta\theta}} - \frac{2}{P}\, \boldsymbol{B} \right)^{-1} \quad (41)$$

where $\boldsymbol{B}$ has bounded entries, and corresponds to the cross terms between the angle and moment estimation errors. If the quantity $(2/P)\boldsymbol{B}$ were to vanish sufficiently quickly, then $\boldsymbol{J}_{\boldsymbol{\theta\theta}} \to \tilde{\boldsymbol{I}}_{\boldsymbol{\theta\theta}}^{-1}$. Interestingly enough, this does not happen for the ARP. The contribution of cross terms does indeed saturate quickly, but the asymptotic bounds do not, in general, converge to the known object moment bounds. We will explore this phenomenon numerically in Section VI.

C. CBP Reconstruction with Angular and Translational Uncertainty

Although more sophisticated methods exist for reconstructing an object from a finite set of parallel beam projections, the CBP method is invariably the benchmark against which any new method is tested. As such, it is an excellent means of examining the effects of angular and translational uncertainty on the reconstruction.

Consider the CBP reconstruction of $f \in L_2(\mathbb{B}_2)$ from a *noiseless* shifted sinogram $\tilde{g} \in \{L_2(\mathbb{B})\}^P$ at a set of angles $\hat{\boldsymbol{\theta}}$ and shifts $\hat{\boldsymbol{\delta}}$ estimated from the *noisy* sinogram $\hat{\tilde{g}}$. We choose to reconstruct from $\tilde{g}$ as opposed to $\hat{\tilde{g}}$ because we wish to study the effects due solely to the angular and shift uncertainties. Defining the angle error as $\varepsilon_i = \theta_i - \hat{\theta}_i$, and the shift error as $t_i = \delta_i - \hat{\delta}_i$, we model the covariance of these errors by the CRB, which we expect to be an accurate predictor of performance at sufficiently high SNR. Thus, we model

$$\mathrm{E}\left\{ \begin{bmatrix} \boldsymbol{\varepsilon} \\ \boldsymbol{t} \end{bmatrix} [\boldsymbol{\varepsilon}^T \boldsymbol{t}^T] \right\} = \begin{bmatrix} \boldsymbol{J}_{\boldsymbol{\theta\theta}} & \boldsymbol{J}_{\boldsymbol{\theta\delta}} \\ \boldsymbol{J}_{\boldsymbol{\delta\theta}} & \boldsymbol{J}_{\boldsymbol{\delta\delta}} \end{bmatrix}$$

where each matrix $\boldsymbol{J}_{\cdot\cdot}$ is extracted from the CRB's derived previously.

[4]Strictly speaking, as $P \to \infty$, the estimation problem is no longer parametric, and the CRB is no longer meaningful. However, in this case, we let P go to infinity in the hopes of characterizing the bounds for the very large P that occur in some applications.

Let $h \in \{L_2(\mathbb{B})\}^P$ denote the filtered sinogram, i.e., $h = \tilde{g} \mathbin{\hat{*}} \rho$, where $\hat{*}$ denotes convolution with respect to the first variable, and ρ is the ramp filter (with smoothing) as specified by the CBP inversion formula. Then the object is estimated as

$$\hat{f}(x,y) = \frac{2\pi}{P} \sum_i h(x\cos\hat{\theta}_i + y\sin\hat{\theta}_i + \hat{\delta}_i, i).$$

To proceed, we assume that the angle errors and shift errors are small, and linearize the reconstruction equations about the true set of view angles $\boldsymbol{\theta}$ and the correct shifts $\boldsymbol{\delta}$. The result is the CBP at the correct set of angles plus a term linear in the errors. Taking the variance of both sides yields the following result:

$$\begin{aligned} \mathrm{var}\{(\hat{f} - f)(x,y)\} = \left(\frac{2\pi}{P}\right)^2 \{ & \boldsymbol{c}_1^T(x,y)\boldsymbol{J}_{\boldsymbol{\theta\theta}}\boldsymbol{c}_1(x,y) \\ & + 2\boldsymbol{c}_1^T(x,y)\boldsymbol{J}_{\boldsymbol{\theta\delta}}\boldsymbol{c}_2(x,y) \\ & + \boldsymbol{c}_2^T(x,y)\boldsymbol{J}_{\boldsymbol{\delta\delta}}\boldsymbol{c}_2(x,y)\} \end{aligned} \quad (42)$$

where $\boldsymbol{c}_1 \colon \mathbb{B}_2 \to \mathbb{R}^P$ is a vector-valued function of (x,y) defined as $\boldsymbol{c}_1(x,y,i) = h'(x\cos\theta_i + y\sin\theta_i + \delta_i, i) \cdot (y\cos\theta_i - x\sin\theta_i)$, and $\boldsymbol{c}_2 \colon \mathbb{B}_2 \to \mathbb{R}^P$ is defined by $\boldsymbol{c}_2(x,y,i) = h'(x\cos\theta_i + y\sin\theta_i + \delta_i, i)$ where $h'(s,i) = (\partial h(s,i)/\partial s)$. Note that we assume that ρ is sufficiently smooth to guarantee that h is differentiable.

VI. Feasibility

In this section, we present a very simple algorithm to solve the angle and shift determination problems given the parallel beam projection data. We first, however, explore the various bounds developed in the previous two sections by evaluating them for an analytical phantom under a number of conditions. These numerical results are sufficiently encouraging to motivate the development of an algorithm. We then outline the symmetric nearest neighbor insertion (SNNI) algorithm, along with some empirical and qualitative descriptions of its behavior. It is comprised of a heuristic initialization routine followed by a locally convergent likelihood maximization. The presented algorithm is simple, and demonstrates that object reconstruction in the absence of angular information is feasible.

A. Exploration of Bounds

We use an analytical phantom, illustrated in Fig. 1, composed of rectangular regions and ellipses. The placement of the components within the phantom was designed to demonstrate the errors introduced into the CBP reconstruction by the uncertainty in the view angles and projection shifts. For the sake of brevity and clarity, we explore the bounds using only a few of the many possible relationships between the relevant variables. We examine the effects of the number of projections, and the order of the method on the angle variance for both the known and unknown shift cases. We hope that these will give a general idea of the behavior of the bounds as a function of these quantities. To quantify the effects of noise, we introduce the following definition of projection SNR:

$$\mathrm{SNR} = \frac{\dfrac{1}{P}\displaystyle\sum_{i=1}^{P} \|g(\cdot,i)\|_2^2}{N_0}$$

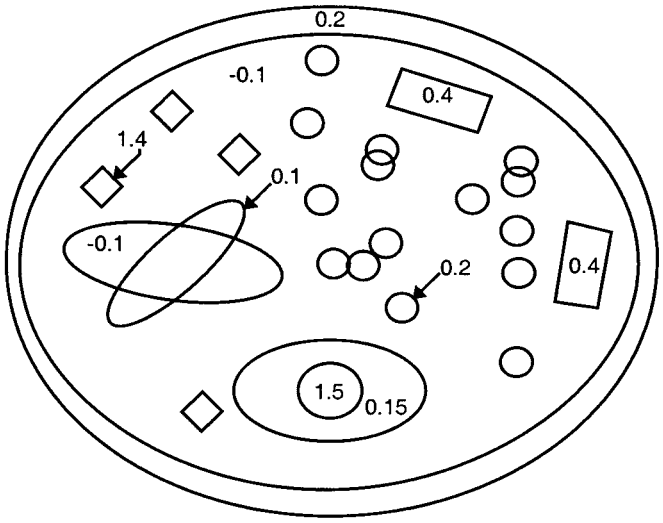

Fig. 1. Analytical phantom used to calculate the various bounds. Objects of the same size and shape have the same density, unless otherwise indicated.

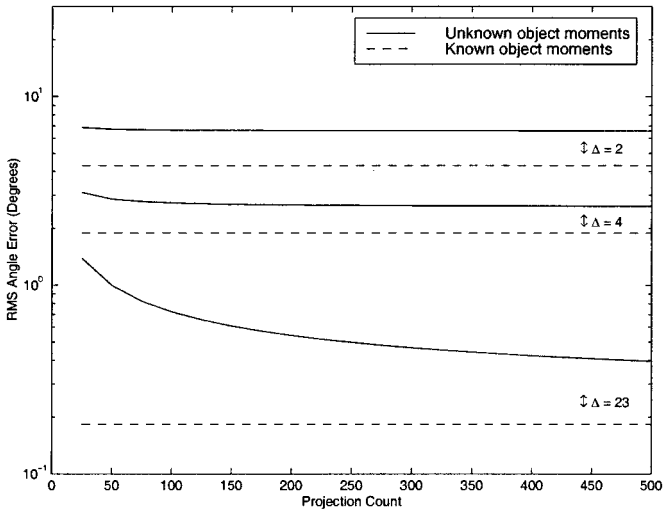

Fig. 3. Comparison of the RMS angle estimation error for the unknown object and known object moment CRB's for $\Delta \in \{2, 4, 23\}$ as a function of P. SNR $= 30$ dB.

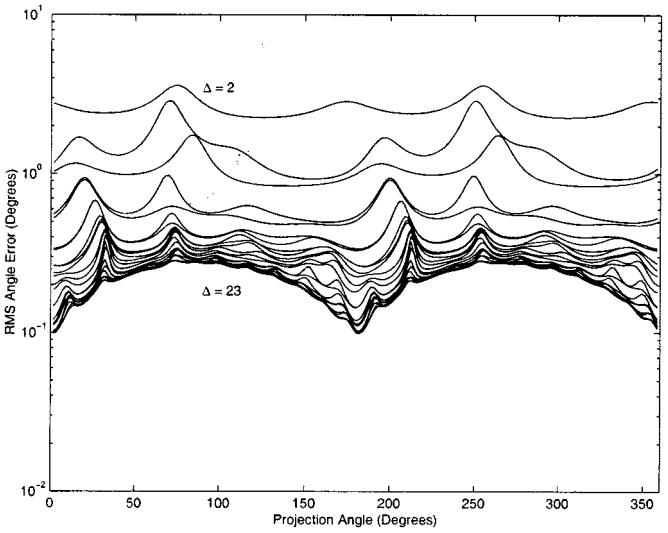

Fig. 2. CRB for RMS angle estimation error in degrees as a function of projection angle for $P = 200$ equally spaced projections with Δ as a parameter taking values in $\{2, \cdots, 23\}$. SNR $= 30$ dB.

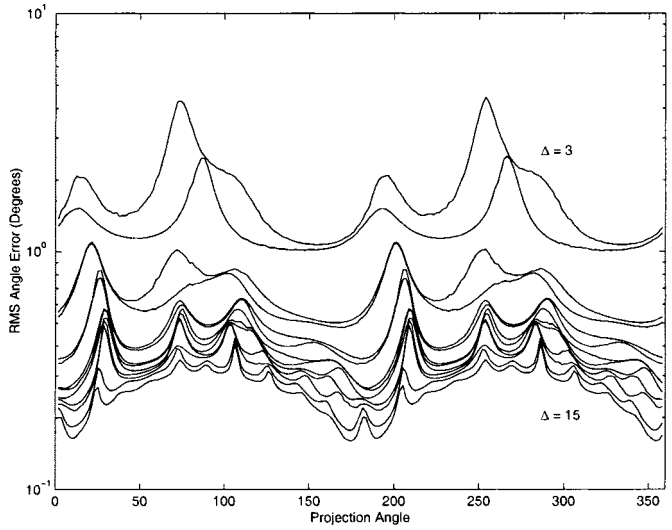

Fig. 4. CRB for RMS angle error as a function of projection angle when estimated jointly with shifts. Here Δ is a parameter, taking values in $\{0, 1, 2, \cdots, n\}$, and $P = 200$. SNR $= 30$ dB.

i.e., as the ratio of the radially averaged projection energy to the noise intensity. Note that in all plots, angles are measured in degrees, and for the sake of simplicity in the interpretation, we have arbitrarily chosen an SNR of 30 dB in Figs. 2–6. The bounds scale linearly with $\sqrt{N_0}$, but this noise level gives a reasonable indication of the kinds of performance that can be expected for this particular phantom.

1) ARP Related Bounds: There are three questions we hope to address via the CRB's computed previously. We will try to answer these questions in the context of the analytical phantom of Fig. 1.

1) How many moments are useful in constructing estimators, i.e., how rapidly does the CRB saturate at Δ is increased for a fixed P?
2) How large (numerically) are the bounds?
3) How does (41) behave as a function of P, i.e., how strongly does P affect the performance?

Fig. 2 addresses the first of these questions for $P = 200$ equally spaced view angles covering the unit circle, and plots the CRB (32) for $\Delta \in \{2, \cdots, 23\}$. Numerical difficulties precluded the calculation of bounds for higher order methods. For this phantom, and this number of projections, the CRB appears to saturate quickly, suggesting little benefit for significantly higher order methods. Fig. 2 also addresses the second question, indicating an RMS error bound of less than 1 degree under these conditions. This suggests that the ARP for this object can be feasibly solved for an SNR ≥ 30 dB.

Fig. 3 addresses the third question, plotting (32) and the known object moment CRB (40) as joint functions of P and Δ. Fig. 3 shows rapid convergence of the bounds as a function of P. For lower order methods, the convergence appears to be far more rapid than for higher order methods. Furthermore, there is a (small) gap between the apparent asymptote of (32) and the known object bound (40). As we mentioned earlier, this is a

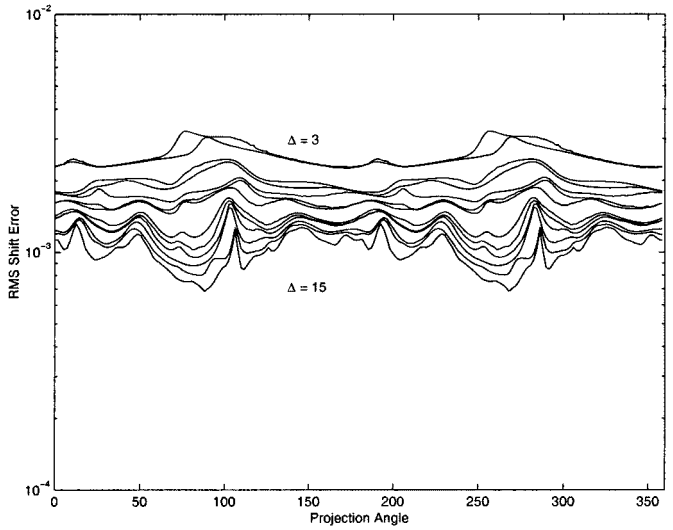

Fig. 5. CRB for RMS shift error as a function of projection angle when estimated jointly with angle. Here $\Delta \in \{3, \cdots, 15\}$ is a parameter, and $P = 200$. SNR = 30 dB.

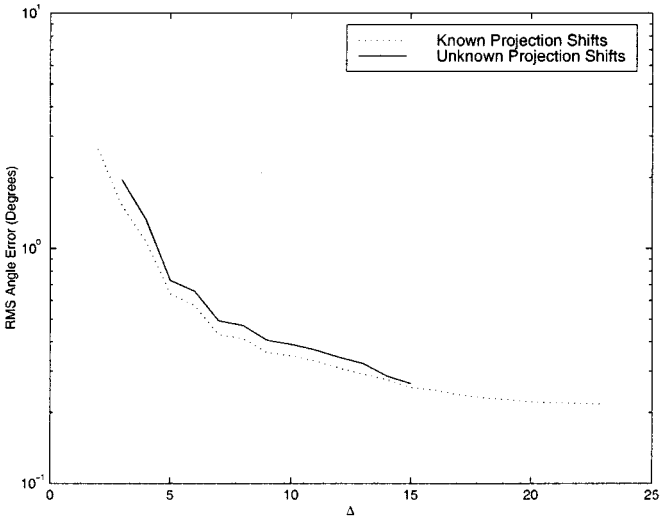

Fig. 6. Comparison of CRB for RMS angle error for the case of known and unknown projection shifts for various choices of Δ, with $P = 200$. SNR = 30 dB.

result of the cross terms between the moments and projections not vanishing as $P \to \infty$.

SHARP Related Bounds: For the SHARP, we have two primary concerns, which we will attempt to address in the context of the analytical phantom of Fig. 1.

1) How large (numerically) are the bounds?
2) How do the bounds on the estimation error of the view angles compare to those for the ARP? In other words, what is the penalty for the additional translational uncertainty in the projections?

Figs. 4 and 5 depict the CRB for the angle and shift errors respectively for $\Delta \in \{3, \cdots, 15\}$ with $P = 200$ equally spaced angles covering the unit circle. The bounds for both the shifts and view angles appear quite reasonable for this phantom and this distribution of view angles.

Fig. 6 clarifies the relationship between the ARP bounds and the SHARP bounds. The RMS angle estimation error is plotted as a function of Δ for both the ARP and the SHARP. For even relatively low Δ, we see that the gap in performance between the two estimators is below 1 dB. We can conclude that for this phantom, very little performance is lost in having to solve the SHARP as opposed to the ARP.

B. Symmetric Nearest Neighbor Insertion (SNNI) Algorithm

The results of the previous subsection are sufficiently encouraging that we have developed a simple algorithm to estimate the angles. The algorithm is separated into three steps:

1) initial shift estimation;
2) projection ordering;
3) joint ML refinement of angles and shifts.

For the sake of simplicity, we first outline the algorithm for the known shift case.

The primary assumption made in the construction of the SNNI algorithm is that the projection angles were chosen independently from a uniform probability distribution on the unit circle, and can therefore be assumed to be approximately equally spaced. This leads to the sub-problem of projection association, in which the projection angles are known, and the projections must be matched to their corresponding view angles. If the angles are sufficiently closely spaced, and the projections sufficiently slowly varying with view angle, then we expect that a nearest neighbor type ordering scheme (such as is used to obtain approximate solutions to the Traveling Salesman Problem) should work reasonably well.

We present such a scheme for step 2 of the algorithm, in which projections are ordered in a greedy fashion by a nearest neighbor selection process. Our variation on the standard Nearest Neighbor Insertion [15] orders the projections on $[0, \pi]$, utilizing the fact that the projections should obey $g(s, \theta + \pi) = g(-s, \theta)$ to flip projections with view angles in $[\pi, 2\pi]$ (something the algorithm must determine). In practice, we order the Legendre moment vectors $\boldsymbol{y}_i$, defined in (23), instead of the projections, because they vary more slowly as a function of view angle. Hence, we also compute the Legendre moment vectors $\boldsymbol{y}_i^R$ of the reversed version of each projection:

$$\boldsymbol{y}_i^R(j) = \int P_{k_j} \hat{g}(-s, i)\, ds, \qquad k_j \in D, k_j < k_{j+1}.$$

Finally, we add some smoothing capability to the NNI in an attempt to increase robustness to errors. The algorithm is detailed in Table I. Note that an implementation of the SNNI algorithm does not need to manipulate the projections $g(s, i)$, but can instead simply manipulate pointers that index the projections, and binary flags that indicate if the projection is to be flipped or not. For our experiments, we chose smoothing factors $\rho_i(n)$ that gave exponential smoothing, normalized so that $\sum_{n=1}^{i} (\rho_i(n))^2 = 1$

$$\rho_i(n) = \frac{\sqrt{1-\alpha^2}\alpha^{i-n}}{\sqrt{1-\alpha^{2i}}}$$

with α chosen (arbitrarily) to be 0.7.

Once the association problem has been solved by the SNNI algorithm, the angle estimates are refined using a

TABLE I
PSEUDO-CODE DESCRIPTION OF THE SNNI ALGORITHM

1. Choose a seed $j \in A \triangleq \{1, 2, \ldots, P\}$. Delete that projection from the list $A \leftarrow A \setminus \{j\}$.
2. Create the output $h \in \{L_2(\mathbb{B}_{\neq})\}^P$ and initialize $h(s,1) \leftarrow \hat{g}(s,j)$. Create the P storage vectors $\boldsymbol{b}_i \in \mathbb{R}^{|D|}$ and initialize $\boldsymbol{b}_1 \leftarrow \boldsymbol{y}_j$. Let $i \leftarrow 1$.
3. While $A \neq \emptyset$ (i.e. unordered projections remain)
- Compute a smoothed moment vector: $\boldsymbol{b}^\star \leftarrow \sum_{n=1}^{i} \rho_i(n)\boldsymbol{b}_n$.
- Find closest vector to $\boldsymbol{b}^\star$ among $\boldsymbol{y}_n, n \in A$:

$$t_1 \leftarrow \min_{n \in A} \|\boldsymbol{b}^\star - \boldsymbol{y}_n\| \qquad m_1 \leftarrow \arg\min_{n \in A} \|\boldsymbol{b}^\star - \boldsymbol{y}_n\|.$$

- Find closest vector to $\boldsymbol{b}^\star$ among $\boldsymbol{y}_n^R, n \in A$:

$$t_2 \leftarrow \min_{n \in A} \|\boldsymbol{b}^\star - \boldsymbol{y}_n^R\| \qquad m_2 \leftarrow \arg\min_{n \in A} \|\boldsymbol{b}^\star - \boldsymbol{y}_n^R\|.$$

- Assign moment vector most similar to $\boldsymbol{b}^\star$ to $\boldsymbol{b}_{i+1}$, and output the appropriate projection:

$$\boldsymbol{b}_{i+1} \leftarrow \begin{cases} \boldsymbol{y}_{m_1} & \text{if } t_1 < t_2 \\ \boldsymbol{y}_{m_2}^R & \text{otherwise} \end{cases} \qquad h(s, i+1) \leftarrow \begin{cases} \hat{g}(s, m_1) & \text{if } t_1 < t_2 \\ \hat{g}(-s, m_2) & \text{otherwise} \end{cases}$$

- Delete projection from available list A, and increment i

$$A \leftarrow \begin{cases} A \setminus \{m_1\} & \text{if } t_1 < t_2 \\ A \setminus \{m_2\} & \text{otherwise} \end{cases} \qquad i \leftarrow i + 1$$

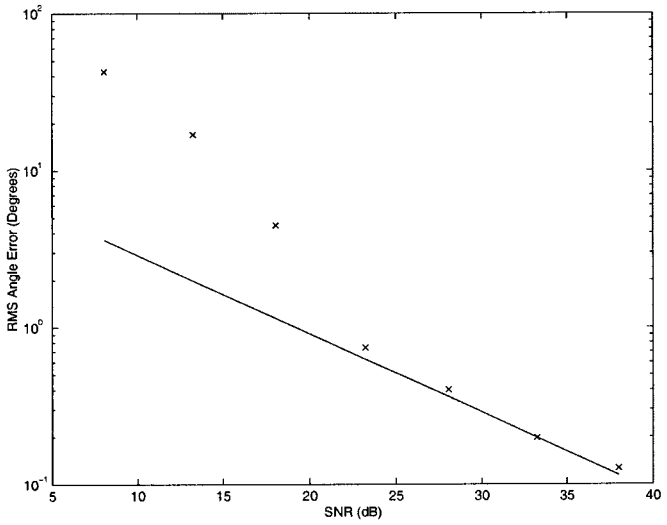

Fig. 7. Comparison of RMS estimation error of the SNNI algorithm to the CRB as a function of projection SNR for phantom shown in Fig. 1. Results shown with $\Delta = 10$ for $P = 100$ uniformly chosen random view angles.

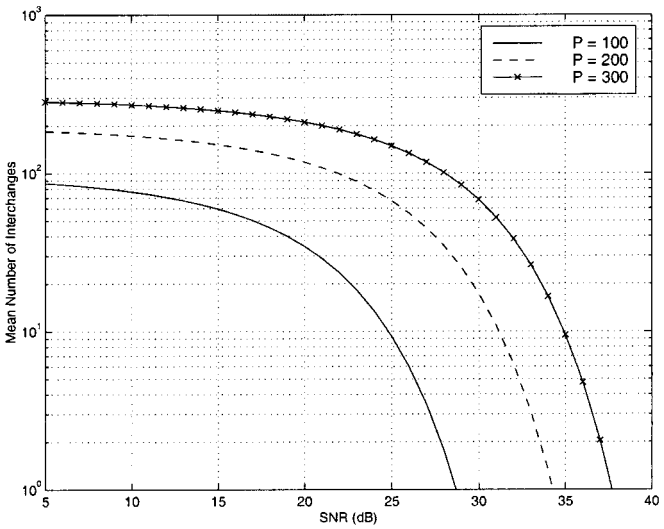

Fig. 8. Mean number of interchanges as a function of projection SNR as predicted by the CRB and an i.i.d. normal distribution on the view angle estimation errors. The sharp drop in the vicinity of an SNR of 15–20 dB for $P = 100$ provides some evidence that the deviation of the SNNI performance from the CRB is a fundamental limitation of the problem, and not a failure of the SNNI. All remaining parameters were the same as those used in Fig. 7.

pseudo-Newton optimization method applied to the concentrated likelihood functional (38). In general, the projection shifts are also unknown. In such cases, the shifts are first estimated by shifting the center of mass of each projection to the origin[5]. This estimation step is generally accurate enough to permit the second step, that of projection ordering, to succeed. The concentrated likelihood $\|\boldsymbol{P}_{\boldsymbol{\Xi}(\boldsymbol{\theta},\boldsymbol{\delta})}\hat{\tilde{\boldsymbol{y}}}\|^2$ is then maximized (again, using a pseudo-Newton method) jointly with respect to angles and shifts.

[5]From the arguments of Section III-C, it follows that we can assume that the object to be estimated belongs to F_2. Thus, the center of mass of the object can be assumed *a priori* to lie at the origin.

C. Simulations

For the simulation, $P = 100$ random view angles were independently chosen from a uniform probability distribution on $[0, 2\pi)$. The SNNI algorithm performed quite well over a range

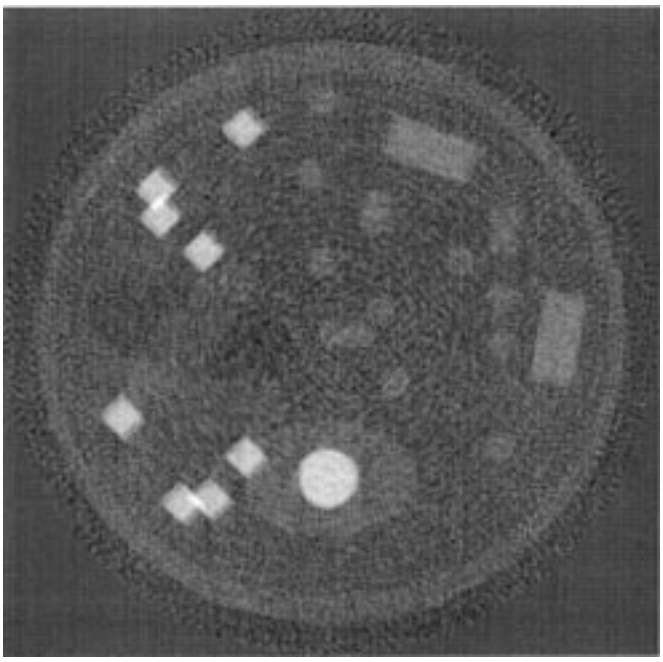

Fig. 9. Reconstruction at 20dB using estimated angles only, to qualitatively demonstrate the noise level below which the proposed SNNI algorithm deviates from the CRB.

of SNR's. Fig. 7 presents the results of Monte Carlo simulations for $\Delta = 10$ in which the algorithm performance is averaged over 100 noise realizations. No simulations were marked as outliers. Numerically, the algorithm appears to achieve the CRB for SNR greater than about 20 dB. The sudden drop in performance at lower SNR may be due to a failure of the algorithm, or due to a threshold effect inherent in the nonlinear estimation problem [16].

To explore this later possibility, we can compute a simple figure of merit from the CRB that suggests the presence of a threshold effect. Intuitively, we expect that algorithm performance should be "poor" (i.e., deviate from the CRB) when the probability that the projections are ordered correctly using the best possible estimator becomes "small." We can approximately quantify this relationship by using the CRB. To do so, we will count the mean number of "interchanges," where an interchange is defined as the event that $|\hat{\theta}_i - \theta_i| > \gamma_i$ where

$$\gamma_i = \tfrac{1}{2} \min_{j \neq i,\, j \in I} |\theta_j - \theta_i|.$$

Thus, an interchange occurs when the estimate $\hat{\theta}_i$ deviates far enough from θ_i that it is now closer to some other view angle θ_j.

We can compute a distribution for the number of interchanges from the CRB. Note that the CRB defines an inverse relationship between the SNR and the angle error variance, so that the rms estimation error is given by $\text{rms}(\hat{\theta}_i - \theta_i) \geq \rho/\sqrt{\text{SNR}}$. If we then assume that the true estimation errors are i.i.d. random variables that are normally distributed with mean 0 and standard deviation $\rho/\sqrt{\text{SNR}}$, we can then calculate the probability of an interchange as $2[1-\Phi(\gamma_i\sqrt{\text{SNR}}/\rho)]$, where $\Phi(\cdot)$ is the standard normal cumulative distribution function. If we also assume that the γ_i's are equal, i.e., $\gamma_i = \gamma$, and that the probabilities of each angle i undergoing an interchange are independent, then we arrive at a binomial distribution for the number of interchanges. Furthermore, the mean number of interchanges is simply

$$\text{E}\{\text{Number of Interchanges}\} = 2P\left[1 - \Phi\left(\frac{\gamma\sqrt{\text{SNR}}}{\rho}\right)\right].$$

For the simulation results depicted in Fig. 7, $P = 100$. Because the angles were randomly chosen, the γ_i are not equal, but for the purposes of this calculation, it suffices to take $\gamma = 1.8$ degrees, which is the mean value of γ_i. With these quantities, and the value of ρ calculated from the CRB for the SHARP, we arrive at the solid line in Fig. 8. Here, the sharp threshold in the mean number of interchanges as a function of SNR is apparent. Furthermore, the threshold occurs in the vicinity of 20 dB, which is where the proposed algorithm begins to deviate significantly from the CRB. Although this fails to provide a theoretically sound reason for the threshold, it does seem to point to an inherent threshold as the reason for the breakdown in performance. As a final demonstration, Fig. 9 depicts an example of a reconstruction at the estimated angles at a noise level of 20 dB, near the vicinity of the threshold. All images presented in this paper have been nonlinearly transformed (i.e., a nonlinear grey-scale map was used) to emphasize small density details. When presenting multiple images of the same nature, the same transformation was used on each image to facilitate comparison.

In performing simulations, we have noted the interesting fact that performance of the SNNI algorithm generally degrades as the number of projections increases. This phenomenon is opposite of the CRB bounds, which decrease as the projection count is increased. On the other hand, if we replot the mean number of interchanges as above for $P = 200$ and $P = 300$, then we arrive at the remaining lines in Fig. 8. For these curves, the threshold has moved to progressively higher SNR's with larger P, indicating that more projections should make estimation at any fixed SNR "harder." We expect such a shift in the threshold from Fig. 3, in which the rapid saturation of the CRB as a function of moment order is apparent. Hence, increasing P fails to significantly change ρ, and instead decreases $\gamma = 180/P$, or equivalently, scales $\sqrt{\text{SNR}}$. This has the effect of shifting the curves in Fig. 8 to the right as P increases. Thus, as in the case of the deviation from the CRB as a function of SNR, the problem of poor SNNI performance with increasing P may not be a true breakdown of the algorithm, but rather a fundamental limitation of the problem.

As a final demonstration of feasibility, we apply the full SNNI algorithm (i.e., we solve the SHARP), to projections computed from three different computer phantoms with significantly different characteristics. For all three phantoms, the projections were chosen uniformly on the unit circle, and randomly shifted. The first is the analytical phantom used thus far with $P = 180$. The second phantom is a smoothed noise field, again with $P = 180$. The third phantom is an MRI brain scan, with $P = 200$. All three simulations were done with an SNR of 40 dB.

In Fig. 10, the simulation results of the SNNI with $\Delta = 10$ have been depicted for all three of the phantoms. For comparison purposes, we have depicted the CBP reconstructions of the phantoms at the correct angles, as well as the standard deviation field of the CBP as calculated in (42) depicted in the rightmost

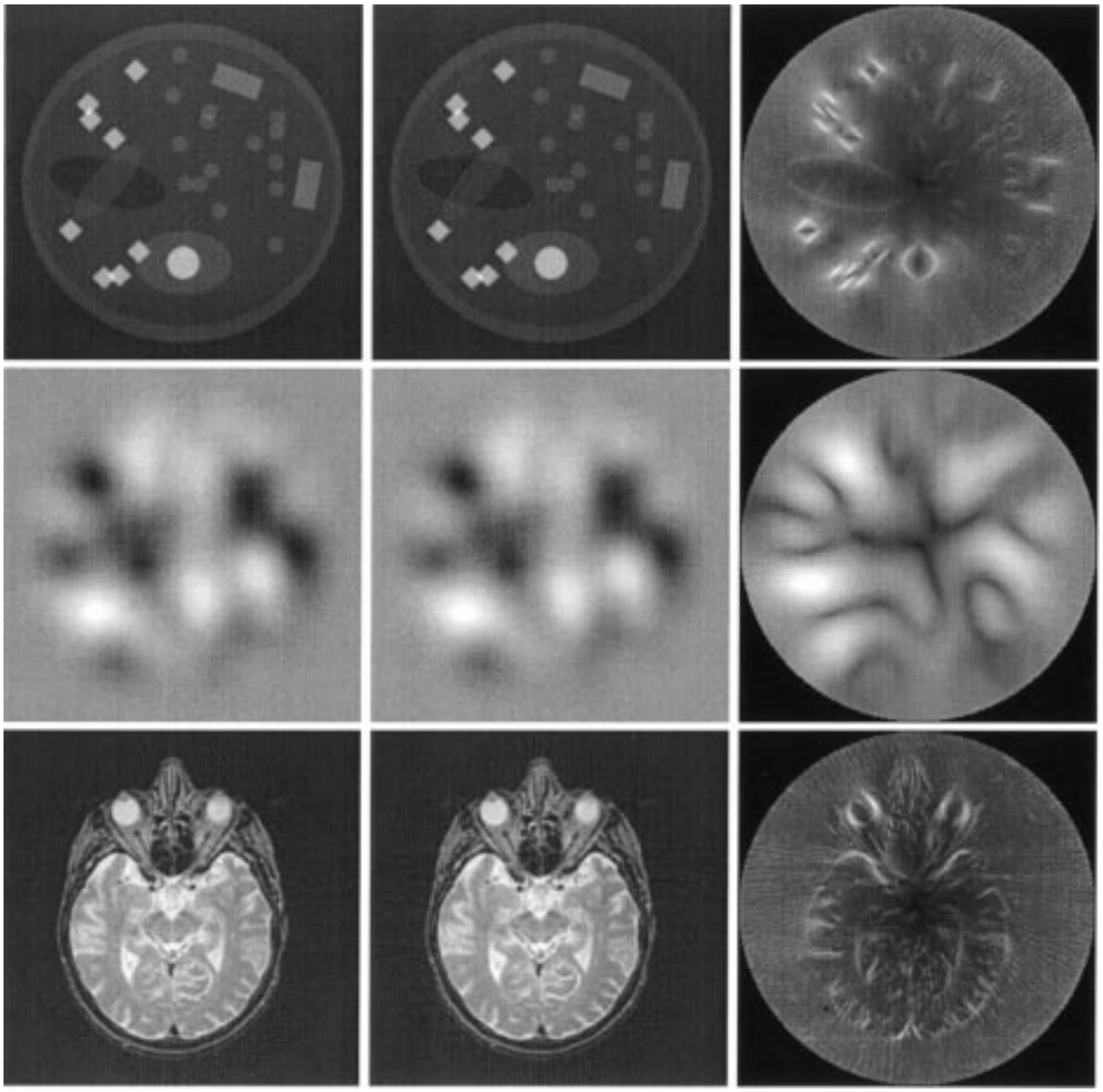

Fig. 10. From left to right, the CBP at the correct shifts and angles, the CBP at the estimated shifts and angles, and the analytical CBP standard deviation field. From top to bottom, the geometric phantom, a smooth random phantom, and a brain scan. All three experiments performed at SNR $= 40$ dB using SNNI ordering and $\Delta = 10$. See text for P.

column. In Fig. 11, we depict the absolute error of the CBP reconstructions of the noiseless projections (to emphasize errors due to misalignment only) using the estimated angles and shifts, averaged over 100 noise realizations. The good agreement between Fig. 11 and the standard deviation field for the geometric phantom in Fig. 10 supports our conclusion that the analytical error field is a good predictor of errors in the reconstruction on average. For a single realization, however, the errors can deviate from their predicted values.

In general, the reconstructions with estimated angles and shifts are visually nearly indistinguishable from the known angle and shift reconstructions. The two types of reconstructions are likewise visually indistinguishable in plots of slices through the reconstruction, which are therefore omitted. Both the error fields and the variance field show blurring along the edges aligned with rays through the reconstruction origin. The smooth noise image has no sharp edges, and thus provides no visual cues for comparison between the known and unknown view angles and shifts case.

VII. Conclusion

In this paper we have demonstrated that the problem of 2-D parallel beam tomography with unknown view angles is stable under very weak conditions. We have developed performance bounds on unbiased estimators, and presented numerical results that suggest that estimation can be done quite well in general. Encouraged by these results, we have constructed a simple heuristic algorithm based on a nearest neighbor type ordering of the projections followed by local

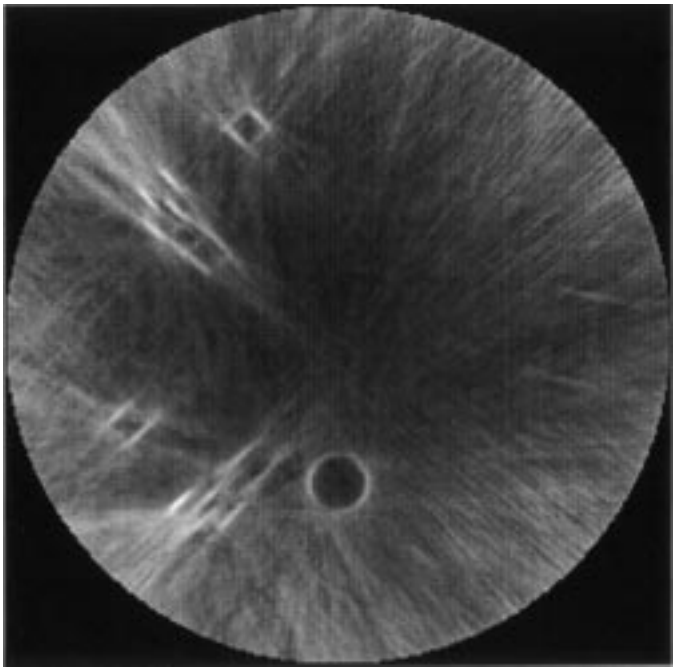

Fig. 11. Absolute error field of the CBP of the noiseless projections at the angles and shifts estimated at SNR = 40 dB by the SNNI algorithm with and $\Delta = 10$. The error field has been averaged over 100 noise realizations.

maximization of the likelihood function. Simulation results on a trio of phantoms demonstrate that this heuristic algorithm performs quite well at moderate SNR. Feasibility of solving the view angle problem at lower SNR's, which may be of interest in high noise applications such as EM based tomography, PET or SPECT, requires further study. A heuristic analysis suggests that performance at lower SNR may be limited by an inherent threshold effect. However, rigorous study of this question and experiments with more powerful algorithms will be needed to determine the actual lowest feasible operating SNR. In any event, based on the results presented in this paper, it should be possible to construct more powerful algorithms that work under varying distributions of the view angles, and to apply the method to real data in a practical situation.

Appendix I
Proof of Theorem 2

Proof: By [2, Theorem 9 and Corollary 5], it follows that if

$$\det \begin{bmatrix} m_{1,0}^2 & m_{2,0} & 1 \\ 2m_{1,0}m_{0,1} & m_{1,1} & 0 \\ m_{0,1}^2 & m_{0,2} & 1 \end{bmatrix} \neq 0 \tag{A.1}$$

and

$$\theta_i \neq \arg\left(\pm \sqrt{\frac{-m_{1,0} - jm_{0,1}}{m_{1,0} - jm_{0,1}}} \right) \tag{A.2}$$

then the ARP has a unique solution to within an equivalence class, i.e., if

$$\mathcal{Q}_d(\hat{\theta}_i; \hat{\boldsymbol{m}}) = \mu_d(i) \qquad d \in \{0,1,2\}, i \in \{1,2,\cdots,P\} \tag{A.3}$$

then

$$\theta_i = \sigma\hat{\theta}_i + c + 2\pi n_i \qquad n_i \in \mathbb{Z} \tag{A.4}$$

for $\sigma \in \{-1,1\}$, $c \in \Omega$. Suppose we now restrict to objects in F_1. Then $\boldsymbol{m} \in W_1$, and $m_{0,1} = 0$, and (A.1) simplifies to

$$m_{1,0} \neq 0, \quad m_{1,1} \neq 0 \tag{A.5}$$

whereas (A.2) simplifies to

$$\theta_i \notin \left\{ \frac{\pi}{2}, -\frac{\pi}{2} \right\}. \tag{A.6}$$

The set S' of objects in F_1 for which $\boldsymbol{m}$ satisfies (A.5) is a $\{0,1,2\}$-generic subset of F_1.

Now, by (A.3) and Theorem 1, it follows that

$$\begin{bmatrix} \hat{m}_{1,0} \\ \hat{m}_{0,1} \end{bmatrix} = \sigma \begin{bmatrix} \cos(c) & \sin(c) \\ -\sin(c) & \cos(c) \end{bmatrix} \begin{bmatrix} m_{1,0} \\ m_{0,1} \end{bmatrix}.$$

But $\boldsymbol{m}, \hat{\boldsymbol{m}} \in W_1$ implies that $\sigma = 1$, $c = 0$. Thus by (A.4), $\boldsymbol{\theta} = \hat{\boldsymbol{\theta}}$, and the ARP admits a unique solution for all $\boldsymbol{m} \in S'$. Furthermore, the set S of objects in F_1 defined in Theorem 2, such that the ARP admits a unique solution contains S', and is thus also a $\{0,1,2\}$-generic subset of F_1. ■

Appendix II
Proof of Theorem 3

Proof: By [2, Theorem 10 and Lemma 12], it follows that if

$$m_{1,1} \neq 0 \quad \text{or} \quad m_{2,0} - m_{0,2} \neq 0 \tag{B.1}$$

$$3\,\text{atan}\left(\frac{m_{1,2} + m_{3,0}}{m_{0,3} + m_{2,1}} \right) - \text{atan}\left(\frac{3m_{1,2} - m_{3,0}}{m_{0,3} - 3m_{2,1}} \right) \neq 0 \tag{B.2}$$

$$\tilde{\mathcal{Q}}_3(\theta_i; \boldsymbol{m}) \neq 0 \tag{B.3}$$

$$U(\theta_i, \rho) \neq 0, \quad U(\theta_i, -\rho) \neq 0 \tag{B.4}$$

where

$$U(\theta,\rho) = c^{j\theta}(\rho^3 c_1 - c_1^*) + \rho(\rho^3 c_1 + \rho^2 c_2 - \rho c_2^* - c_1^*)c^{j2\theta} + \rho^5 c_1 - \rho^2 c_1^* \tag{B.5}$$

$$c_1 = \tfrac{1}{8}[(m_{3,0} - 3m_{1,2}) + j(m_{0,3} - 3m_{2,1})]$$
$$c_2 = \tfrac{3}{8}[(m_{3,0} + m_{1,2}) + j(m_{0,3} + m_{2,1})] \tag{B.6}$$

and

$$\rho = \sqrt{\frac{m_{2,0} - m_{0,2} + j2m_{1,1}}{m_{2,0} - m_{0,2} - j2m_{1,1}}}. \tag{B.7}$$

Then the SHARP has a unique solution to within an equivalence class, i.e., $\exists \delta_x, \delta_y \in \mathbb{R}$, $\sigma \in \{-1,1\}$, $c \in \Omega$ such that for all $i = 1, \cdots, P$,

$$\hat{\delta}_i = \delta_i + \delta_x \cos\theta_i + \delta_y \sin\theta_i$$

and

$$\theta_i = \sigma\hat{\theta}_i + c + 2\pi n_i$$

for some $\delta_x, \delta_y \in \mathbb{R}$, $c \in \Omega$, $\sigma \in \{-1,1\}$. Suppose we now restrict to W_2. Then (B.1) and (B.4) simplify to

$$m_{2,0} - m_{0,2} \neq 0$$

and

$$U(\theta_i, 1) \neq 0, \quad U(\theta_i, -1) \neq 0$$

respectively. Now, let S' be the set of $\boldsymbol{m} \in W_2$ that satisfy these conditions. Then it is simple to show that S' is the intersection of a finite number of $\{0, 1, 2, 3\}$-generic sets, and is thus $\{0, 1, 2, 3\}$-generic. Furthermore, in the same manner as the Proof of Theorem 2, it follows that for $\boldsymbol{m} \in S'$, the SHARP has a unique solution, i.e., $\hat{\boldsymbol{\delta}} = \boldsymbol{\delta}, \hat{\boldsymbol{\theta}} = \boldsymbol{\theta}$. Finally, the set S of objects in F_2 defined in Theorem 3, such that the SHARP admits a unique solution, contains S', and is thus also a $\{0, 1, 2, 3\}$-generic subset of F_2. ■

REFERENCES

[1] S. R. Deans, *The Radon Transform and Some of Its Applications*. New York: Wiley, 1983.

[2] S. Basu and Y. Bresler, "Uniqueness of tomography with unknown view angles," *IEEE Trans. Image Processing*, vol. 9, pp. 1094–1106, June 2000.

[3] M. Hedley and H. Yan, "Motion artifact suppresson: A review of post-processing techniques," *Magn. Reson. Imag.*, vol. 10, pp. 627–635, 1992.

[4] R. Ehman and J. Felmlee, "Adaptive technique for high-definition MR imaging of moving structures," *Radiology*, vol. 173, pp. 255–263, Oct. 1989.

[5] M. Wood, M. Shivji, and P. Stanchev, "Planar-motion correction with use of k-space data acquired in Fourier MR imaging," *J. Magn. Reson. Imag.*, vol. 5, pp. 57–64, Jan. 1995.

[6] T. Sachs, C. Meyer, P. Irarrazabal, B. Hu, D. Nishimura, and A. Macovski, "The diminishing variance algorithm for real-time reduction of motion artifacts in MRI," *Magn. Reson. Med.*, vol. 34, pp. 412–422, 1995.

[7] D. Salzman, "A method of general moments for orienting 2D projections of unknown 3D objects," *Comput., Vis., Graph., Image Process.*, vol. 50, pp. 129–156, 1990.

[8] A. B. Goncharev, "Methods of integral geometry and recovering a function with compact support from its projections in unknown directions," *Acta Applican. Math.*, vol. 11, pp. 213–222, 1988.

[9] F. Natterer, *The Mathematics of Computerized Tomography*. New York: Wiley, 1986.

[10] S. Basu and Y. Bresler, "The stability of nonlinear least squares problems and the Cramér–Rao bound," *IEEE Trans. Signal Processing*, to be published.

[11] H. Van Trees, *Detection, Estimation, and Modulation Theory, Part I*. New York: Wiley, 1968.

[12] R. Ash, *Real Analysis and Probability*. New York: Academic Press, 1972.

[13] M. Abramowitz and I. Stegun, *Handbook of Mathematical Functions*. New York: Dover, 1972.

[14] S. Basu and Y. Bresler, "Two theorems on the column rank of certain matrices with trigonometric entries," Coord. Syst. Lab., Univ. Illinois, Urbana–Champaign, Tech. Rep. UILU-ENG-99-2230, 1999.

[15] M. Syslo, N. Deo, and J. Kowalik, *Discrete Optimization Algorithms: With Pascal Programs*. Englewood Cliffs, NJ: Prentice-Hall, 1983.

[16] M. Zakai and J. Ziv, "On the threshold effect in radar range estimation," *IEEE Trans. Inform. Theory*, pp. 167–169, Jan. 1969.

Samit Basu (M'00) received the B.E.E. degree (magna cum laude) from the University of Delaware, Newark, in 1995, and the M.S. and Ph.D. degrees in electrical engineering from the University of Illinois, Urbana-Champaign, in 1998 and 2000, respectively.

In 2000, he joined the General Electric Corporate Research and Development Center, Niskayuna, NY, where he is currently an Electrical Engineer working on problems in tomographic reconstruction and signal processing.

Dr. Basu is the recipient of the Eugene DuPont Scholarship; a graduate fellowship from the Electrical and Computer Engineering Department, University of Illinois; a graduate fellowship from the Joint Services Electronics Program; and the Mac VanValkenburg Memorial Fellowship.

Yoram Bresler (F'99) received the B.Sc. (cum laude) and M.Sc. degrees from the Technion, Israel Institute of Technology, Haifa, in 1974 and 1981, respectively, and the Ph.D. degree from Stanford University, Stanford, CA, in 1985, all in electrical engineering.

From 1974 to 1979, he was an Electronics Engineer in the Israeli Defense Force. From 1979 to 1981, he was a Consultant with the Flight Control Laboratory, Technion, developing algorithms for autonomous TV aircraft guidance. From 1985 to 1987, he was a Research Associate with the Information Systems Laboratory, Stanford University, working on sensor array processing and medical imaging. In 1987, he joined the University of Illinois, Urbana-Champaign, where he is currently a Professor with the Department of Electrical and Computer Engineering and the Bioengineering Program, and a Research Professor with the Coordinated Science Laboratory. In 1995–1996 he spent a sabbatical leave at the Technion. His current research interests include multidimensional and statistical signal processing and their applications to inverse problems in imaging and sensor arrays. He is currently on the editorial board of *Machine Vision and Applications.*

Dr. Bresler was an Associate Editor for the IEEE TRANSACTIONS ON IMAGE PROCESSING from 1992 to 1993, and a member of the IEEE Image and Multidimensional Signal Processing Technical Committee from 1994 to 1998. In 1988 and 1989, he received the Senior Paper Awards from the IEEE Acoustics, Speech, and Signal Processing Society. He is the recipient of a 1991 NSF Presidential Young Investigator Award, the Technion Fellowship in 1995, and the Xerox Senior Award for Faculty Research in 1998. In 1999, he was named a University of Illinois Scholar.